



HAL
open science

Characteristic Textures of Recrystallized, Peritectic, and Primary Magmatic Olivine in Experimental Samples and Natural Volcanic Rocks

Saskia Erdmann, Bruno Scaillet, Caroline Martel, Anita Cadoux

► **To cite this version:**

Saskia Erdmann, Bruno Scaillet, Caroline Martel, Anita Cadoux. Characteristic Textures of Recrystallized, Peritectic, and Primary Magmatic Olivine in Experimental Samples and Natural Volcanic Rocks. *Journal of Petrology*, 2014, 55 (12), pp.2377-2402. 10.1093/petrology/egu060 . insu-01089999

HAL Id: insu-01089999

<https://insu.hal.science/insu-01089999>

Submitted on 2 Dec 2014

HAL is a multi-disciplinary open access archive for the deposit and dissemination of scientific research documents, whether they are published or not. The documents may come from teaching and research institutions in France or abroad, or from public or private research centers.

L'archive ouverte pluridisciplinaire **HAL**, est destinée au dépôt et à la diffusion de documents scientifiques de niveau recherche, publiés ou non, émanant des établissements d'enseignement et de recherche français ou étrangers, des laboratoires publics ou privés.

Characteristic textures of recrystallized, peritectic, and primary magmatic olivine in experimental samples and natural volcanic rocks

Saskia Erdmann, Bruno Scaillet, Caroline Martel, Anita Cadoux

1 Université D'Orléans, ISTO, UMR 7327, 45071 Orléans, France

2 CNRS, ISTO, UMR 7327, 45071 Orléans, France

3 BRGM, ISTO, UMR 7327, BP 36009, 45060 Orléans, France

Corresponding author: serdmann@dal.ca

Suggested running title: Textures of recrystallized, peritectic, and primary magmatic olivine

ABSTRACT

Olivine textures are potentially important recorders of olivine origin and crystallization conditions. Primary magmatic and xenocrystic origins are commonly considered for olivine from ultramafic to intermediate magmas, while secondary olivine origins (i.e. crystals formed by recrystallization or peritectic reaction) are rarely considered in the interpretation of magmatic phenocrysts. The main aim of our study was to determine textures that are characteristic for secondary magmatic olivine and non-characteristic, or at least rare, for primary magmatic olivine. To characterize the textures of the different olivine types, we review previous experimental work and present new textural data for olivine from four melanorite melting and eight basalt crystallization experiments. We (i) qualitatively characterize olivine textures using transmitted light and back-scattered electron microscopy; and (iii) semi-quantitatively characterize the 2D surface area of olivine branches and individual crystals, their 2D and calculated 3D shapes, and 2D grain boundary segment

lengths. Olivine recrystallization yields crystals dendritic branches, while peritectic reaction produces olivine cluster with randomly oriented crystals. In agreement with previous studies, we find that olivine crystal and branch size, grain boundary segmentation, and inclusion relations cannot unequivocally distinguish between olivine of secondary and primary origins. However, recrystallized olivine typically has short prismatic branches, while primary magmatic olivine dendrites commonly have elongated branches. The peritectic crystals closely compare to glomerocrysts and individual polyhedral primary magmatic crystals, but they commonly form small groups of touching crystals and cluster with crystal-poor cores. Spatial association and a comparison with xenocrysts textures may further guide the interpretation of their origin, but detailed analyses of core compositions and zoning patterns appear necessary to firmly distinguish peritectic from primary magmatic crystals. Our comparison of experimental and natural samples suggests that dendritic olivine crystals and cluster of polyhedral olivine that commonly occur in mafic and ultramafic igneous rocks should be evaluated for possible primary as well as secondary magmatic origins.

Keywords: olivine; crystal cluster; dendritic; peritectic; primary magmatic; secondary magmatic; recrystallization; texture;

INTRODUCTION

Olivine is a characteristic primary phase in ultramafic to intermediate magmas recrystallization ($\text{liquid1} \rightarrow \text{olivine1} + \text{liquid2}$), but also commonly forms xenocrysts, thus yielding information on the open- and closed-system evolution of magma systems (e.g., Donaldson, 1974; Helz, 1987; Costa & Dungan, 2005; Arndt *et al.*, 2010; Qian & Hermann, 2010; Erdmann *et al.*, 2012; Famin *et al.*, 2009; Welsch *et al.*, 2013). Secondary olivine formed by recrystallization ($\text{olivine1} + \text{liquid1} \rightarrow \text{olivine2} + \text{liquid2}$) or by peritectic replacement of mafic precursor minerals (e.g., $\text{orthopyroxene} + \text{liquid 1} \rightarrow \text{olivine2} + \text{liquid 2}$) has been produced in experiments (e.g., Brearley & Scarfe, 1986; Tsuchiyama, 1986; Boudier, 1991; Erdmann *et al.*, 2012; Jacobs, 2012). They form dendritic crystals and cluster of subhedral-euhedral, randomly oriented crystals, respectively (Fig. 1). Few examples of possible olivine recrystallization (Boudier, 1991; Dunworth & Wilson, 1998; Arndt *et al.*, 2010) and peritectic crystallization (Erdmann *et al.*, 2010, 2012) have also been reported from natural samples, but these origins are rarely considered in interpreting the textures and compositions of olivine phenocryst.

Differences in crystal size may discriminate between olivine of various origins in mixed crystal populations (e.g., Dunworth & Wilson, 1998; Amma-Miyasaka & Nakagawa, 2002; Costa & Dungan, 2005; Arndt *et al.*, 2010), but size is not an independent criterion for interpreting olivine origin. Rounded and embayed olivine grain boundary segments may be evidence for partial dissolution (Donaldson, 1985; Tsuchiyama, 1986; Helz, 1987; Boudier, 1991), but they may also be primary growth features (Donaldson, 1976; Moore & Erlank, 1979; Welsch *et al.*, 2013; Faure & Schiano, 2005). Euhedral grain boundary segments may be most characteristic for primary magmatic growth, but they also form by recrystallization; peritectic growth, or late-stage epitactic overgrowth (Boudier, 1991; Arndt *et al.*, 2010;

Erdmann *et al.*, 2010). Deformation features, such as microfractures, subgrains, and deformation twins have been taken to infer a xenocrystic origin of olivine crystals in many examples (e.g., Helz, 1987; Boudier, 1991; Dunworth & Wilson, 1998; Vinet & Higgins, 2010), and they may identify restitic cores of recrystallized olivine. However, olivine deformation has also been inferred to take place during compaction of crystal mush or magmatic flow (e.g., Clague & Denglinger, 1994; Natland, 2003), and lattice mismatch as a result of dendritic growth has further been inferred to resemble deformation textures (Sunagawa, 2005; Welsch *et al.*, 2013). Exotic inclusions (i.e. inclusions that differ from the cognate melt composition and/or mineral assemblage) may reflect primary crystallization resulting from local supersaturation (Maaløe & Hansen, 1982; Faure & Schiano, 2005; Roeder *et al.*, 2006), but they may also be relics of xenocrystic assemblages or dissolution and reprecipitation (Thornber & Huebner, 1985; Helz, 1987; Dungan & Davidson, 2004; Erdmann *et al.*, 2012).

It thus appears that few, if any, of the commonly considered olivine textures can unequivocally discriminate crystals of primary magmatic from those of secondary magmatic origin. The main aim of our study was to identify textures that are characteristic for secondary (recrystallized or peritectic olivine) and – at least – rare for primary magmatic olivine crystallized directly from the melt. We hypothesized that such textures exist, as the components (olivine, reactive mafic phase, and/or melt) and processes (one- or multi-phase dissolution-reprecipitation versus primary crystallization) of crystallization strongly differ. For example, “dusty-“, “sieve-“, or “cellular-textured” plagioclase, clinopyroxene, orthopyroxene, or spinel crystals are commonly inferred to form by dissolution-reprecipitation (e.g., Tsuchiyama, 1985; Johannes *et al.*, 1994; Streck, 2008), and they are texturally distinct from primary magmatic crystals of the same mineral types.

To examine potentially characteristic textures of secondary and primary magmatic olivine, we (i) review previous experimental studies on secondary, recrystallized and peritectic olivine; (ii) present new textural data on olivine crystal size, shape, and grain boundary segmentation for recrystallized and peritectic olivine produced in melanorite melting experiments (in which rock powders were partially melted); and (iii) compare this data to primary magmatic olivine crystallized in new and published crystallization experiments (in which glasses were partially crystallized). We propose that crystal and branch shape may be the best criteria to distinguish between secondary, recrystallized olivine and primary magmatic olivine dendrites. Cluster shape and crystal orientation within clusters appear the best textural criteria to distinguish secondary, peritectic and primary magmatic, glomerocrystic olivine. We conclude with an evaluation of possible natural examples from the Tataro-San Pedro volcanic complex in Chile, and literature examples in which olivine forms dendritic crystals and cluster of subhedral-euhedral, randomly oriented crystals.

FORMATION OF SECONDARY OLIVINE IN PREVIOUS EXPERIMENTS

Textures of experimentally recrystallized and peritectic olivine have been described by a limited number of studies. Tsuchiyama (1986) has performed reaction experiments between olivine and SiO₂-rich host melts that yielded recrystallized, Fo-rich vermicular crystals (Fig. 1a). Natural olivine crystals were used as starting material, cut into cubes with variable crystallographic orientation and then pressed into pellets with andesite and boninite rock powders. These pellets were then heated to temperatures between 1100 and 1321°C in an atmospheric gas-mixing furnace. Dissolution and recrystallization of \leq Fo₃₉ olivine yielded vermicular crystals resembling dusty-, sieve-, and fingerprint-textured plagioclase (Fig. 1a)

Boudier (1991) has characterized textures of partially recrystallized olivine (Fig. 1b,c) from a plagioclase lherzolite that was partially melted and deformed using a Griggs press. The melting experiment was performed under 5% constant strain and a confining pressure of 0.7 MPa. Partial melting and olivine recrystallization took place at ~1500 to ~1650 °C. Inclusion-rich olivine recrystallized to undeformed, euhedral branches in optical continuity with their restitic cores. The breakdown of the cores commenced along (100) and (001) planes. Recrystallization proceeded by growth of (010) and {110} blades that in cases showed minor orientation mismatch between neighbouring units. Euhedral branches reached lengths of ~50-200 μm and axial a:b:c ratios of ~1.2:1.0:1.5 (Fig. 2 and Table 2 of Boudier, 1991). Boudier highlighted the low shape anisotropy of the recrystallized olivine branches compared to primary magmatic dendrites crystallized at high growth rates, but she considered substructures (e.g, inclusions) as the best criteria for distinguishing primary dendritic olivine from dendritic crystals with a secondary origin.

We have previously presented textural data for peritectic olivine formed by partial melting of melanorite and leuconorite rock powders (Fig. 1 d; Erdmann et al. 2012). The experiments were performed in internally heated pressure vessels at 200 MPa and temperatures between 1000 and 1150 °C. The peritectic olivine crystals replaced amphibole, orthopyroxene, and phlogopite of the starting materials. They formed clusters with euhedral to subhedral, randomly oriented crystals. Olivine replacing orthopyroxene yielded clusters with high olivine proportions and relatively large crystals (top Fig. 1d). Olivine replacing amphibole and phlogopite yielded clusters with relatively small olivine crystals and high or low olivine proportions (bottom Fig. 1d).

NEW DATA AND METHODS

As detailed in the following sections, we (i) have used transmitted light and BSE images for the qualitative comparison of olivine textures, and (ii) present measurements of the 2D surface area, 2D and 3D shape analysis, and 2D grain boundary segmentation of olivine branches and peritectic crystals. Our melting experiments used rock powders that were partially melted to produce secondary olivine. As detailed below, we report results for one new melanorite melting experiment (MN2-12) and new data for three additional melanorite melting experiments (MN-2, MN-9, and MN-12) of Erdmann *et al.* (2012) (Table 1). Our crystallization experiments employed a glass starting material that was then partially crystallized. For primary magmatic olivine formed in the crystallization experiments, we report phase assemblage, 2D surface area, and 2D and 3D shape analysis for eight basalt crystallization experiments (B-1 to B-12; Table 1). Experiments with variable temperature (1000-1150 °C) and H₂O content (0.5-4.2 wt% added) were examined to compare textures of the different olivine types over a range of crystallization conditions. The new MN2-12 melting experiment was performed with a more mafic and unaltered starting material than that of the MN melting experiments to test for effects of compositional variation of the original assemblages on the resulting olivine textures.

Starting materials

Raw starting materials for our experiments were a basalt (B) from the Upper Placeta San Pedro sequence of the Tatara-San Pedro volcanic complex of the Southern Volcanic Zone in Chile, and two melanorite xenoliths (MN and MN2) recovered from dacitic lavas of the complex (whole-rock compositions are given in Table 2). Geochemical and stratigraphic details of the Tatara-San Pedro volcanic complex and important contaminants are reported by

Dungan *et al.* (2001) and Costa *et al.* (2002) and references therein. The major constituents of the MN xenolith are plagioclase (~60 vol%; predominantly ~An₈₀), amphibole (~13 vol%; X_{Mg} ~77), orthopyroxene (~7 vol%; ~En₇₈, Fs₂₀, Ws₂; X_{Mg} ~80), phlogopite (~3 vol%; X_{Mg} ~80), olivine (~15 vol%; ~Fo₈₀), and oxides (~2 vol%). Most olivine has iddingsite rims, microfractures, and oxide inclusions. The major constituents of the MN2 xenolith are plagioclase (~40 vol%; ~An₈₂ core composition), olivine (~20 vol%; ~Fo₇₇), orthopyroxene (~15 vol%; ~En₇₉, Fs₁₉, Ws₂; X_{Mg} ~80), amphibole (~15 vol%; X_{Mg} ~78), phlogopite (~6 vol%), and Cr-spinel (~4 vol%). The MN2 olivine has a slightly lower Fo content than in the MN starting material (~Fo₇₇ versus ~Fo₈₀), but is unaffected by alteration. The basalt starting rock contains phenocrysts and xenocrysts of plagioclase (~10 vol%), olivine (~5 vol%), and clinopyroxene (~3 vol%) set in a matrix composed of plagioclase, olivine, clinopyroxene, orthopyroxene, and oxides.

The coarse-grained MN and MN2 starting rocks were separately crushed to experimental starting material powders of $\leq 170 \mu\text{m}$ that consisted of crystal and few rock fragments. The starting material of the basalt crystallization experiments was a glass fused twice for ~4 h at 1400 °C and atmospheric conditions. Between and after fusing, the glass was ground to $< 20 \mu\text{m}$ in an agate mortar.

Experimental methods

All experiments were performed with an internally-heated pressure vessel at the Institut des Sciences de la Terre d'Orléans, France. Pressure was obtained by sequential loading of a mixture of H₂ and Ar gas at room temperature (Scaillet *et al.*, 1995). Charges were then heated at a rate of 10-15 °C/min from room temperature to ~40 °C below the experimental temperature. Final heating was performed at 2-4 °C/min to minimize overstepping of set point temperatures to $\leq 10 \text{ °C}$ for $\leq 10 \text{ min}$. The experiments were ended by drop quench (e.g.,

Di Carlo *et al.*, 2006). Experimental fO_2 was calculated from Ni–Pd–NiO solid sensors using the calibration of Pownceby & O'Neill (1994). Several fragments from different parts of the experimental charges were first mounted in epoxy resin and polished for BSE imaging and microprobe analysis. Following electron beam analysis, thin sections were then prepared from the sample mounts.

Experimental conditions

All experiments were performed at ~200 MPa at temperatures of 1000 and 1150 °C with ~0.5 and 4.2 wt% H₂O added to the charges as summarized in Figure 2 and Table 1. The analyzed MN melting experiments were selected from those presented by Erdmann *et al.* (2012). The run products of three experiments were chosen for further analyses according to (i) the presence of recrystallized olivine (MN-2 and MN-12), and (ii) crystallization at a range of crystallization temperatures and intermediate to high experimental H₂O contents (Fig. 2a,b). One run product, in which olivine showed pervasive recrystallization, was selected from a series of experiments with the MN2 starting material to test the effect of variable rock and olivine composition on olivine textures. The analyzed B crystallization experiments were chosen, because they cover a range of olivine textures.

The average experimental fO_2 was NNO+0.7. Gold capsules were used as sample containers for experiments at 1000 and 1043 °C; Au₈₀Pd₂₀ capsules were used for experiments at 1085 and 1150 °C. Calculated experimental Fe loss was -39 to -23 % relative for the 1150 and 1085 °C experiments, but less than -15 % relative for the ≤ 1043 °C experiments. This limits the application of our compositional data (summarized in the Electronic Appendix) and affected the location and size of mineral stability fields (e.g., expanding the stability field of olivine), but the main insights gained from our textural analysis remain applicable, as both melting and crystallization experiments experienced Fe

loss. If olivine textures were affected, it was the case for crystallization of secondary and primary magmatic olivine.

All melting experiments and the examined crystallization experiments were performed at sub-liquidus conditions (Fig. 2), which allowed us to limit experimental Fe loss. However, the crystallization experiments therefore contained abundant nuclei when they reached the target P-T values, particularly in low-temperature, low-H₂O experiments (in which dissolution of nuclei was inefficient). The experimental conditions that yielded specific olivine growth morphologies thus cannot be used to infer the intensive crystallization parameters (magmatic temperature or H₂O content) of natural magmas containing olivine with equivalent morphologies. Nevertheless, in combination with textural observations from published experiments with supra-liquidus heating, we can use our results to infer characteristic features of primary versus secondary olivine.

The experimental run times were 21, 23, to 24 hours for the melting experiments and 19, 26, and 41 h for the crystallization experiments. These variations in run times preclude a direct comparison of the textures produced at specific run durations. However, the run durations of the melting and crystallization experiments overlap, which allows us to qualitatively assess the effects of time, temperature, and experimental H₂O on olivine textures and the importance of these parameters compared to the processes of secondary versus primary crystallization on the considered textures.

Olivine classification

To quantitatively analyze olivine textures we have first classified recrystallized and peritectic olivine in MN and MN2 melting experiments as summarized in Figures 3 and 4a. Olivine in MN and MN2 melting experiments with core compositions equivalent to crystals of the starting material is classified as restitic (Ol-R). Subhedral to euhedral olivine in optical

continuity with restitic crystal cores is classified as recrystallized (Ol-RC). The main evidence that these olivine zones are recrystallized portions of restitic crystals is the partial preservation of original olivine compositions in the cores of some branches, though epitactic crystallization may have contributed to their crystallization (i.e. by $Ol1+L1 \rightarrow Ol2+L2$). Inclusion-poor and randomly oriented olivine in crystal clusters or small groups are classified as peritectic (Ol-P). To further distinguish different types of peritectic olivine we have followed the classification of Erdmann *et al.* (2012) summarized in Figure 3, but we have renamed the olivine types. We distinguish peritectic olivine formed after amphibole (Ol-P-Amp), orthopyroxene (Ol-P-Opx), and phlogopite (Ol-P-Phl) according to olivine proportions in clusters, crystal sizes, and grain boundary segment lengths. Olivine produced in the basalt crystallization experiments is referred to as primary magmatic (Ol-PM).

Textural analysis

In addition to the qualitative descriptions, we have characterized the 2D branch and/or crystal surface area, the 3D shape, the 2D maximum major and minor axial lengths, and grain boundary segment (GBS) lengths (Fig. 4). We consider the textural data to be semi-quantitative, because small crystals (commonly $\leq 15 \mu\text{m}$ in length) were measured, the size of our datasets is limited (Table 3; $n=43-305$ for 2D surface area and 3D shape; $n=244-468$ for GBS lengths), and sectioning effects may have played a role. We nevertheless consider that the data illustrate first order similarities and differences in textures between secondary and primary experimental olivine crystals.

The textures and phase distributions of the run products of the crystallization experiments are relatively homogeneous and crystal orientations are random. Textures and phase distribution of the run products of the melting experiments are more heterogeneous, reflecting the use of rock powders as starting materials, but crystal orientations also appear

random (Fig. 5). Crystal accumulation in parts of the experimental charges was not detected. For recrystallized olivine we have measured branches of 5 to 10 crystals per charge (e.g., Fig. 4 b,c). For primary magmatic olivine we have analyzed between ~90 and 300 polyhedral crystals or 2D intersections of olivine branches per charge. For peritectic olivine we have measured crystals from 3 to 6 crystal clusters (Table 3). As peritectic crystals commonly form sub-clusters of touching grains that lack visible grain boundaries in BSE images (e.g., C2 as compared to C1 in Fig. 4b,d), we have drawn their outlines using BSE images and then used transmitted light microscopy to estimate their actual size and shape (Fig. 4d).

Crystals of each olivine type were analyzed from different parts (i.e. fragments) of the experimental charges. Drawings of 2D branches and crystals (Fig. 4c,d) were subsequently converted into binary images and analyzed using the SCION image software to quantify their 2D surface area and the 2D major and minor axial lengths. The 2D major and minor axes of olivine branches and crystals were further used to characterize their 3D shape employing the CSDslice spreadsheet of Morgan & Jerram (2006) (Fig. 4e). In addition to the calculated 3D values, we present “maximum” 2D major/minor axial ratios determined using the ten largest values derived from our image analysis. The correspondence between major, intermediate, and short axes of olivine and the crystallographic a,b,c directions are unconstrained. The 2D grain boundary segment (GBS) length, taken as the length of euhedral GBSs between inflection points, was measured in CoreIDRAW (Fig. 4f).

The estimated standard errors for the 2D surface area and the 2D GBS length are <6 and <2 % of the population range. The reported reliability of the shape estimate (R^2) is the fractional measure of the variation in the sample explained by the best-fit shape of the database. We acknowledge that additional, unconstrained errors relate to the small crystal size and the choice of sections analyzed (e.g., we may have inadvertently analyzed more core

zones of peritectic crystal clusters for one charge than for another), and that the textural data should therefore be considered as semi-quantitative.

Bulk, mineral, and glass compositions

Whole-rock starting materials reported in Table 2 were analyzed using a Phillip's PW2400 X-ray spectrometer at the Regional Geochemical Centre of Saint Mary's University, Halifax. Olivine and glass compositions reported in the Electronic Appendix were determined using a JEOL 8200 electron microprobe at Dalhousie University, Canada. Core-rim zoning with increasing and decreasing in X_{Mg} [$Mg/(Mg+Fe) \times 100$] is referred to as reverse and normal, respectively. The mineral abbreviations used follow those of Whitney & Evans (2010).

EXPERIMENTAL RESULTS

In the following sections, we first describe the textures of restitic, partially recrystallized and peritectic olivine formed in our melting experiments and then present a textural overview of primary magmatic olivine formed in previous and in our crystallization experiments. We then summarize the effects of variable experimental temperature, H_2O content, and olivine composition on the textures of the different olivine types.

Melanorite melting experiments

Restitic and recrystallized olivine

Partial melting of the two melanorite starting materials produced between ~12 and 3 wt % restitic olivine (OI-R) and ~2 to 8 wt% recrystallized olivine, decreasing in abundance with increasing experimental temperature and H_2O content and from MN2 to MN experiments (Fig. 2 a; Table 1). The restitic crystals have irregular shapes, reminiscent of the crystal

fragments that were added to the charges (Figs 5, 6). Their cores commonly contain some nanopores or healed microfractures (e.g., Fig. 6a,e,f) and they have on average Fo₈₀ and Fo₇₇ composition in MN and MN2 experiments, respectively, equivalent to olivine of the starting materials (the compositions are summarized in the Electronic Appendix). Zoning from restitic cores to recrystallized rims is normal and relatively sharp in 1000 °C experiments (Fig. 6d,e) to reverse and gradational in ≥ 1085 °C experiments (Fig. 6f-i).

The restitic crystals in the 1000 °C and 1085 °C experiments typically show minor resorption in the form of regularly embayed grain boundaries as well as subhedral grain boundary segments (e.g., Ol-R in Fig. 6d). However, some restitic crystals are rimmed by zones of optically continuous, recrystallized branches (Fig. 6a) that partially preserve the composition of the original restitic crystal and nano-inclusions in their cores. Restitic crystals in the 1150 °C experiments have sub-rounded shapes and they are partially, but pervasively resorbed (Fig. 6g-i). They show abundant glass-filled channels and pores that deeply intersect the restitic cores (e.g., Fig. 6g,h). Their grain boundary segments are curved to euhedral. As in the low-temperature experiments, some of the olivine crystals show branches that are in crystallographic continuity with the restitic cores (Fig. 6b,c). Nanopores are rare in their cores, while compositions of the original restitic olivine are partially preserved in the cores of some branches.

The axes of elongation of the recrystallized olivine branches is typically subparallel (Fig. 6g,h), although marginal branches often show a preferred shape orientation subparallel to the margin of the crystals (e.g., Fig. 6i). We also note that the major axes of elongation of the restitic fragments and their branches commonly appear to have oblique orientations (e.g., Fig. 6h versus 6g). The 2D surface area of the recrystallized branches commonly reaches up to $\sim 200 \mu\text{m}^2$ and $\sim 1000 \mu\text{m}^2$ in low- and high-temperature experiments, while the average 2D surface areas range between $\sim 110 \mu\text{m}^2$ and $\sim 940 \mu\text{m}^2$ (Fig. 7a-c; Table 3). The 2D cross-

sections of the olivine branches have short prismatic shapes with calculated axial ratios of ~1.0 to 1.0-1.1 to 1.3-1.4 (Fig. 8a-c). The average 2D GBS lengths of the recrystallized branches range between ~3 and 8 μm (Fig. 9a-c; Table 3).

Peritectic olivine

Partial melting of the MN and MN2 starting materials yielded between ~25 and 4 wt% peritectic olivine, decreasing in abundance with increasing experimental temperature and H₂O content and from MN2 to MN experiments (Fig. 2b; Table 1). Crystals are largely unzoned with ~Fo₉₁ to ~Fo₇₆ composition in 1150 and 1000 °C experiments, respectively (Electronic Appendix). Crystal cluster consist of <10 to >100, sub-radially to randomly oriented crystals (Fig. 10). Crystals commonly seem to be organised around a large central glass pool (e.g., Fig. 5b, 10b). Sub-groups of touching crystals that form cluster with compact to elongated shapes are common (Fig. 10a-e). The crystals have variable optical orientation, but their grain boundaries are often invisible in BSE images (e.g. Figs 4b,d and 10b). The shape and size of the peritectic crystal clusters are variable, resembling the variable size and shape of crystal fragments added to the charges.

Peritectic olivine formed after orthopyroxene (Fig. 10a,b) typically forms clusters that are composed of single crystals enveloped by glass or by subgroups of two to a few touching individuals. The crystals have average 2D surface areas between ~150 and 240 μm^2 and commonly reach maximum 2D crystal sizes of up to ~500 μm^2 (Fig. 7d-g; Table 3). The Ol-P-Opx crystals are short prismatic with axial ratios of ~1.0 to 1.2-1.4 to 1.3-1.6 (Fig. 8d-g). Their average 2D GBS lengths range between ~3 μm and ~7 μm (Fig. 9d-g). The Ol-P-Opx crystals are thus smaller than the branches of recrystallized olivine formed at 1150 and 1085 °C and larger than recrystallized olivine branches formed at 1000 °C, but their morphologies and 2D GBS lengths closely compare to those of recrystallized olivine. In contrast, olivine

formed after amphibole (Fig. 10c,d) typically forms clusters of typically >50 variably oriented, touching crystals. Individual crystals have mean and maximum 2D crystal sizes of $\sim 45 \mu\text{m}^2$ and $<150 \mu\text{m}^2$ (Fig. 7h; Table 3). The crystals are short prismatic with axial ratios of ~ 1.0 to 1.2 to 1.3 (Fig. 8h). The mean GBS length of Ol-P-Amp branches is $\sim 4 \mu\text{m}$ and few GBSs are $>12 \mu\text{m}$ long (Fig. 9h). The Ol-P-Amp crystals are thus smaller and have shorter 2D GBSs than the Ol-P-Opx crystals. They also form larger subgroups of touching crystals. Lastly, olivine formed after phlogopite (Fig. 10e,f) has 2D surface areas of $<200 \mu\text{m}^2$ and typically $<100 \mu\text{m}^2$ (Fig. 7i; Table 3). The crystals are acicular with axial ratios of ~ 1.0 to 1.1 to 3.0 (Fig. 8i). The mode of 2D GBS lengths is $\sim 4 \mu\text{m}$, while most 2D GBSs are $<12 \mu\text{m}$ long (Fig. 9i). The acicular shape clearly distinguishes Ol-P-Phl from Ol-P-Opx and Ol-P-Amp crystals (Fig. 8i versus 8d-h).

Primary magmatic olivine

Published crystallization experiments with intermediate to ultramafic starting materials and sub-liquidus as well as supra-liquidus heating histories have produced olivine with polyhedral to variably skeletal and hopper-shaped to dendritic morphologies (e.g., Donaldson, 1976; Lofgren, 1989; Faure *et al.*, 2007; Shea & Hammer, 2013). Typical examples reported by Donaldson (1976) are summarized in Figure 11, which show that the polyhedral, skeletal and hopper-shaped crystals have short prismatic morphologies (Fig. 11a-d), while the dendritic crystals have moderately to strongly elongated branches and crystal shapes (Fig. 11e-g). The first-order branches of dendritic crystals are oriented parallel to the major elongation of the crystals, while lower-order branches are curved and may have oblique orientations (Fig. 11g).

The crystallization of basaltic glass in our 1000 to 1085 °C experiments yielded ~ 4 to 18 wt% olivine, decreasing in abundance with increasing experimental temperature and H₂O content (Fig. 2c; Table 1). Olivine forms the largest crystals of the assemblage, ranging in

composition from $\sim\text{Fo}_{72}$ to Fo_{85} . (Figs 5d-f, 12). The crystals have smaller sizes and apparently short prismatic and polyhedral morphologies in experiments with 0.5 wt% H_2O added and larger sizes and elongated to dendritic morphologies in experiments with ≥ 2.1 wt% H_2O added (Figs 5 and 12; Table 3). The calculated 3D shapes, however, suggest short prismatic crystal morphologies of $\sim 1.0:1.11:2:1.5-1.9$ for olivine from all experiments (Fig. 13), while the reliability of the shape estimate (R^2) decreases from apparently polyhedral olivine formed in low- H_2O experiments ($R^2 \geq 0.82$; Fig. 13a,b) to those of apparently dendritic crystals in high- H_2O experiments ($R^2 \leq 0.73$; Fig. 13e,h). In contrast, the calculated maximum 2D major/minor axial ratios increase from ~ 2.5 in low- H_2O experiments (Fig. 10 a,b) up to ~ 4.0 in high- H_2O , low-temperature experiments (Fig. 10e), consistent with the macroscopically observed textures (Figs 12 and 13). We therefore conclude that the simple 2D analyses are more useful for our characterization of morphologically complex crystals than the 3D estimates.

Effects of experimental conditions and system components on olivine textures

Crystallization temperature, H_2O content, and melanorite starting material compositions were varied to test for possible effects of these parameters on olivine textures. However, the limited number of experiments and their different run times permit only a qualitative evaluation. The relatively small variation in experimental run durations ($\sim 19-42$ hours) had no first-order effect on the analyzed textures (Fig. 14a-c).

Compositional variation exerts important controls on the olivine textures. For branches of recrystallized olivine and peritectic olivine formed after orthopyroxene, the 2D surface area increases from experiment MN-12 with a partially altered assemblage to experiment MN2-12 with an unaltered assemblage and more mafic composition (e.g., Figs 7b,c,e,f and 14). The textures of peritectic olivine are also strongly controlled by their

precursor minerals (Figs 7g-i, 8g-i,9g-i and 10), and likely by the composition of their host melts. However, the compositions of all three olivine types overlap. Recrystallized and peritectic olivine have $\sim\text{Fo}_{91-76}$ and primary magmatic olivine has $\sim\text{Fo}_{85-72}$ composition. The crystallization processes – primary crystallization, dissolution-recrystallization, and peritectic crystallization – and not composition, are thus the primary controls of olivine textures.

For primary magmatic olivine, the 2D surface area tends to increase with decreasing temperature and increasing H_2O content of the experiments (Fig. 14d,e). For peritectic olivine formed after orthopyroxene, the 2D surface tends to increase with decreasing temperature and increasing H_2O content (Fig. 14d,e). For branches of recrystallized olivine, the 2D surface increases from olivine branches formed in low-temperature, high- H_2O experiments to those formed at high-temperature and intermediate H_2O contents (Fig. 14d,g). The 2D GBS lengths of all olivine types appear to increase with experimental temperature and decrease with experimental H_2O content, although the scatter in the datasets is considerable (Fig. 14f,i). The 2D maximum/minimum axial ratios also show minor variation as a function of temperature or H_2O content, but their values are consistently higher for the primary magmatic than for the recrystallized and peritectic olivine crystals.

DISCUSSION OF THE EXPERIMENTAL RESULTS

Experimental approach and conditions

Before proceeding with a discussion of the characteristic textures of secondary and primary olivine, we first examine possible effects of our experimental approach and conditions on olivine textures. As stated above, the variable experimental conditions (Table 1) preclude a detailed comparison of textures for primary and secondary olivine crystallized at equivalent experimental temperature, H_2O , and run duration. However, variations in run duration (~ 19 -

41 hours) had no first-order effect on the examined olivine textures (Fig. 14a-c), and the crystallization temperatures and H₂O contents of our melting and crystallization experiments overlap (Figs 2, 14; Table 1). The data thus allow us to qualitatively compare potentially characteristic textures of the different olivine populations.

The short run durations and sub-liquidus heating of the experiments resulted in the formation of a relatively large number of relatively small crystals (i.e. commonly $\leq 15 \mu\text{m}$ long). As the run durations are shorter than crystallization times in typical natural systems, we anticipate that primary olivine crystals of most natural systems will have significantly larger crystal sizes than those formed in our experiments. Moreover, textures of partial recrystallization as those observed for restitic olivine in our melting experiments may not be preserved for significantly longer reaction times than those of our experiments. Possible effects of continued crystallization and ripening on olivine textures in natural systems need to be furthermore considered.

The constant experimental heat supply may have also affected the formation of specific olivine textures by controlling the rate limiting process in olivine crystallization (e.g., diffusive transfer of components versus growth of dendritic branches through melt boundary layers). These limitations imply that the textures of experimental and natural olivine crystallized at the same temperature, pressure, and H₂O conditions will likely differ, but we maintain that the textures of experimentally produced olivine can guide the interpretation of natural examples if they are sensibly interpreted.

In the following, we first discuss characteristic and potentially distinguishing textures of secondary versus primary magmatic olivine as summarized in Table 4, and then conclude with the discussion of potential natural examples.

Characteristic textures of recrystallized olivine

Characteristic textures of the partially recrystallized olivine crystals in our melting experiments are: (i) the crystallographically continuous, dendritic rims on restitic cores that locally contain healed microfractures and inclusions; (ii) branches with small to large 2D surface areas compared to peritectic olivine; (iii) branches with short prismatic habits; (iv) outer branches with preferred shape orientation subparallel to the margin of the crystals; and (v) commonly oblique orientations between the major axes of elongation of the restitic fragments and their branches (Table 4; Fig. 6). The textures of the partially recrystallized olivine in our experiments closely compare to those reported for recrystallized olivine from previous experimental studies of Tsuchiyama (1986) and Boudier (1991) as summarized in Figure 1. The crystallographically continuous character of the recrystallized olivine branches unequivocally distinguishes them from clusters of peritectic olivine (e.g., Fig. 6a versus Fig. 10a). However, the continuous optical character and other features of the recrystallized, dendritic olivine closely compare those of primary magmatic dendrites. In the following, we therefore evaluate the potential of various textures to distinguish dendritic olivine of secondary, recrystallized and primary magmatic origins.

Inclusions and deformation features

Inclusions and deformation features in restitic cores of partly to largely recrystallized olivine may be a useful criterion for identifying xenocrysts as previously suggested (e.g., Moore & Erlank, 1979; Boudier, 1991; Dunworth & Wilson, 1998; Dungan & Davidson, 2004). However, it has also been argued that microfractures may form by magmatic deformation or around inclusions (Natland, 2003; Welsch *et al.*, 2013). Infilling of skeletal cavities or space between dendritic, primary magmatic crystals during late-stage crystallization may further mimic healed microfractures (Maaløe & Hansen, 1982; Roeder *et al.*, 2006), while primary

magmatic dendritic growth has been invoked to explain sub-grain textures and orientation mismatch between dendritic branches (Natland, 2003; Sunagawa, 2005; Welsch *et al.*, 2013).

Abundant fluid-filled nanopores present in some restitic cores of the recrystallized olivine in our experiments (e.g., Fig. 6 e,f) are interpreted as relics of decomposed iddingsite. Inclusions of this type are obvious and are important evidence for the replacement of an altered or hydrous precursor mineral. However, recrystallized antecrysts and most xenocrysts will be devoid of such inclusions or healed microfractures. Euhedral spinel inclusions within some recrystallized olivine branches of our charges (e.g., Fig. 6i) could be derived from the decomposition of original spinel inclusions in contact with melt. It is more likely though that they have formed by dissolution of Cr-rich olivine, orthopyroxene, amphibole, and/or phlogopite and local supersaturation as the spinel crystals show a relatively homogeneous distribution within secondary olivine and its interstitial glass (Fig. 5b). However, supersaturation and crystallization with entrapment of inclusions may equally relate to primary magmatic olivine growth (Maaløe & Hansen, 1982; Roeder *et al.*, 2006; Welsch *et al.*, 2013). In agreement with previous studies we therefore conclude that inclusions in olivine may record important information on crystallization processes, but that they rarely provide unequivocal evidence for a specific origin of their host crystal.

The size and GBS length of dendritic branches

The range in the 2D surface area of the recrystallized olivine branches produced in experiments compares to the size of branches produced in previous experiments (Figs 1 and 6), but also overlaps with sizes of experimentally crystallized primary magmatic olivine (Figs 13 and 14; Table 3). Moreover, dendritic olivine of unequivocally primary origin (e.g., in crusts of pillow basalts or spinifex layers of komatiites) forms micrometre to decimetre-size crystals (e.g., Donaldson, 1976; Natland, 2003; Faure *et al.*, 2006; Mattioli *et al.*, 2006). The

size of dendritic olivine is therefore not a useful criterion to *per se* discriminate olivine of various origins. However, as for recrystallized, cellular-textured plagioclase (cf. Tsuchiyama, 1985; Johannes *et al.*, 1994), we anticipate (i) that the size of recrystallized olivine branches will show a limited range, likely on the scale of micrometres to millimetres; and (ii) that the largest branches will form at high temperature, volatile-rich crystallization conditions, and for originally Fo-rich restitic olivine. For example, we interpret the small recrystallized branches formed in our low-temperature MN melting experiments to reflect the recrystallization of partially altered olivine (iddingsite rims) and the larger subunits to reflect slower dissolution-recrystallization of unaltered olivine in the high-temperature experiments. We therefore suggest that the branch size of dendritic olivine is not a discriminating feature to determine olivine origin, but that branch sizes of secondary olivine may yield important information on recrystallization conditions and the composition of precursor crystals. The length of GBSs of the different olivine types also closely agree, and therefore cannot be used to infer their origins. However, the GBS lengths vary with experimental temperature and H₂O conditions (Fig. 14f,i), and they therefore also record important information on crystallization conditions.

The shape of dendritic crystals

The range in morphologies of the partially recrystallized restitic olivine crystals in our experiments reflects the use of rock- and crystal-fragments as starting materials. Recrystallized xenocrysts and antecrysts derived from fracturing of wall rocks, cumulates, and crystal mush in natural systems may likewise show a large range in shape and sizes. However, irregularly-shaped primary magmatic olivine dendrites may also form, reflecting growth in variable sub-environments or on an irregular substrate (e.g., spinifex crystals in komatiite flows; e.g., Faure *et al.*, 2006). It is also possible that fragmentation during magmatic flow produces irregularly-shaped primary magmatic olivine dendrites (e.g., Clague

& Denglinger, 1994; Natland, 2003). However, it should be feasible to determine whether dendritic crystals fractured, or whether fractured crystals recrystallized into dendritic crystals (e.g., by characterizing zoning patterns). While we conclude that irregular shapes of dendritic olivine provide no unequivocal evidence for secondary versus primary magmatic origins, we consider a detailed analysis of crystal shapes as an important guide for interpreting their crystallization history and origin.

The shape of dendritic branches

The short prismatic shape of recrystallized olivine branches that is characteristic for crystals in our experiments has been previously described by Boudier (1991) (Fig. 1b,c), who suggested that this morphology is typical for recrystallized olivine, but not necessarily evidence for a secondary origin. We concur with this conclusion, but stress that short prismatic branches are a common feature of secondary olivine dendrites, while they appear to be a rare feature of primary magmatic dendrites (e.g., morphologies shown in Fig. 1 versus Fig. 11 or examples shown by Henderson *et al.*, 1986; Faure *et al.*, 2006; O'Driscoll *et al.*, 2007). We therefore suggest that short prismatic branches of dendritic olivine should be considered as possible evidence for a secondary magmatic origin and that particular attention should be paid in the interpretation of olivine phenocrysts with such morphologies.

Optical orientation of dendritic branches

The parallel optical orientation of the main dendritic branches is a common feature of primary and secondary magmatic olivine (e.g., Figs 1a-c and 11). However, dendritic olivine of both origins may also show some optical orientation mismatch between branches. Minor orientation mismatch between neighbouring branches of recrystallized olivine has been described by Boudier (1991; her Fig. 2b). Orientation mismatch and curvature of branches in

primary magmatic olivine has also been documented, but curved branches commonly characterize dendrites crystallized at large degrees of supercooling (e.g., the feather dendrite shown in Fig. 11 g). They are characterized by highly elongated branches and should thus be distinguishable from the short prismatic branches of recrystallized olivine.

Shape anisotropy of dendritic branches

In our experiments, we further observe that the outer branches of recrystallized olivine commonly show a preferred shape orientation subparallel to the margin of the crystal (e.g., Fig. 6i). For plagioclase, similar textures have been observed, reflecting recrystallization subparallel to the dissolution surface of the crystals (e.g., Johannes *et al.*, 1994; e.g., their Fig. 17b). The major axes of elongation of the restitic fragments and their dendritic branches also commonly appear to have oblique orientations. While the recrystallization of irregular olivine fragments should lead to such shape anisotropy between crystals and their branches, it is non-trivial to distinguish true anisotropy from simple sectioning effects (e.g., in our experimental charges an insufficient number of crystals is exposed for statistical analysis). Moreover, primary magmatic olivine dendrites may also show such anisotropies, if they have grown on an irregular substrate, or if they have fractured following initial growth. A detailed analysis of zoning patterns should help to distinguish such primary from secondary growth, but any anisotropy of olivine dendrites needs to be cautiously interpreted.

Characteristic textures of peritectic olivine

Characteristic textures of the peritectic olivine crystals in our melting experiments are: (i) the occurrence in clusters of randomly to sub-radially oriented crystals that commonly show olivine-rich rims and olivine-poor interiors; (ii) the presence of sub-groups of touching crystals that form compact to branch-like groups, where grain boundaries are often invisible in BSE images; and (iii) distinct crystal sizes and habits for peritectic crystals formed after

various precursor minerals (Figs 3 and 10). Their textures compare to those of peritectic crystals formed in other dissolution and melting experiments performed at different pressure and temperature conditions and with variable starting materials (Brearley & Scarfe, 1986; Erdmann *et al.*, 2012; Jacobs, 2012). The peritectic crystal clusters are easily distinguished from primary and secondary magmatic dendritic crystals by their random orientation, but they may be mistaken for primary magmatic glomerocrysts. Moreover, peritectic crystals dispersed by magmatic flow may texturally resemble polyhedral primary magmatic crystals.

Peritectic crystal cluster

Erdmann *et al.* (2012) have suggested that peritectic olivine formed after orthopyroxene, amphibole, and phlogopite can be distinguished from each other on the basis of olivine/glass proportion in clusters, the size of the peritectic crystals, and their GBS lengths. Here, we note that their shape may be a further distinguishing criterion, ranging from acicular for olivine that replaced phlogopite (Figs 8i, 10e,f) to short prismatic forms for olivine that replaced orthopyroxene and amphibole (Figs 8d-h, 10a-d). That the boundaries of touching crystals are commonly invisible in BSE imaging mode (e.g., Figs 4b,d, 10d) may indicate that these clusters commonly contain twins, but it could also reflect polishing effects.

The presence of olivine clusters with variable textures in natural samples may point towards the presence of peritectic crystals replacing more than one primary phase, but texturally variable glomerocrysts or peritectic and glomerocrystic crystal cluster may also be juxtaposed. It is notable that several of the experimental peritectic crystal clusters are zoned from relatively olivine-rich rims to glass-rich interiors with few touching crystals (e.g., Fig. 10a,b), reflecting nucleation of the peritectic crystals on the exterior of the decomposing phases with inwardly directed dissolution and crystallization. Glomerocrysts, in contrast,

typically show outwardly directed growth or random clustering, where crystals commonly touch in the central zones of clusters (e.g., Jerram *et al.*, 2003).

Dispersed peritectic crystals

Dispersed subgroups or individual peritectic crystals in natural samples will texturally resemble primary magmatic olivine. The size, shape, or length of GBSs cannot *per se* be used to distinguish between peritectic and primary magmatic crystals (e.g., Fig. 14). However, the occurrence of xenocrysts or antecrysts may point towards their presence. We moreover consider a textural comparison of potential peritectic crystals and xenocrysts as a useful tool to infer olivine origin. For example, the size of recrystallized olivine branches is larger, while their shape and GBS lengths closely compare to those of experimentally produced peritectic olivine formed after orthopyroxene. If recrystallized olivine can be identified, its textures may guide the interpretation of other olivine populations in the same samples, while a combination with detailed compositional and zoning pattern analysis seems to have the best potential to distinguish peritectic from primary magmatic olivine.

In the following, we discuss possible natural occurrences of secondary magmatic olivine from natural rocks. We first report examples from the Tatara-San Pedro volcanic complex in Chile using our own data. We then review possible literature examples from picrites.

POSSIBLE NATURAL EXAMPLES

Olivine phenocrysts in lavas of the Tatara-San Pedro volcanic complex

Texturally variable olivine phenocrysts are common in many mafic to ultramafic igneous rocks (e.g., Helz, 1987; Boudier, 1991; Costa & Dungan, 2005; Natland, 2003; Welsch *et al.*,

2013). For instance, basaltic-andesitic and andesitic lavas of the Tatara-San Pedro (TSP) volcanic complex contain texturally and compositionally complex populations of olivine xenocrysts (Fig. 15; Dungan & Davidson, 2004; Costa & Dungan, 2005). In addition, the presence of abundant peritectic olivine has been inferred (Erdmann *et al.*, 2010, 2012).

The inferred peritectic olivine forms small clusters or individual crystals (Fig. 15a). The crystals are characterized by a lack of deformation features that are common in olivine xenocrysts, but they commonly show crystallized, exotic melt film pseudomorphs that are interpreted to have formed by partial melting of contaminants (cf. Dungan & Davidson, 2004). The euhedral to subhedral shape of the olivine crystals mimics the shape of experimentally produced peritectic olivine, but they are significantly larger than the experimentally produced crystals. Moreover, reactive minerals including amphibole, phlogopite, and orthopyroxene are common in xenoliths enclosed in dacitic TSP lavas (Costa *et al.*, 2002), but largely absent from xenocrysts assemblages. The main population of the peritectic olivine in our sample set (“Type-2 Ol” of Erdmann *et al.*, 2012) is inferred to have formed after orthopyroxene. New shape data determined using the CSDslice spreadsheet indicate that the crystals approach short prismatic shapes with axial ratios of $\sim 1.0:1.3:1.6$ ($R^2 \sim 0.89$), which is consistent with olivine formation after orthopyroxene. In our sample set, the peritectic crystals also have lower Fo core compositions than the xenocrysts (Fig. 15).

Apparent olivine xenocrysts in our TSP sample set range from macro- to megacrysts (Fig. 15a-c). Most of the olivine crystals show rounded to euhedral grain boundary segments and euhedral-subhedral protrusions (Fig. 15b), which we interpret to reflect marginal dissolution and recrystallization. Few olivine megacrysts show irregular, skeletal to dendritic textures (e.g., Fig. 15c) with short prismatic subunits or branches, which we interpret as partially recrystallized xenocrysts. Rare skeletal-dendritic olivine also occurs in xenoliths, and the megacrysts could thus have recrystallized during xenolith entrainment or subsequent

dispersal in the magmas. They have textures and core compositions that compare to those of olivine from cumulate xenoliths, and they locally show healed microfractures that are also typical for the xenolithic olivine that commonly do not extend into rim zones of the crystals.

Olivine dendrites and cluster in mafic-ultramafic igneous rocks: literature examples

Studies that have previously suggested the presence of secondary, recrystallized olivine in ophiolites, melilitites, kimberlites, and basanitite are those of Boudier (1991), Dunworth & Wilson (1998), Ninomiya & Arai (1998), and Arndt *et al.* (2010). Dunworth & Wilson (1998) have interpreted olivine crystals with mottled textures to record possible replacement of initial xenocrystic cores. Ninomiya & Arai (1998) have presented a detailed investigation of olivine types produced by reaction between peridotite xenoliths and basanite magma. They show that relatively small, subhedral to euhedral, and strain-free olivine crystals with minute spinel inclusions (their olivine phenocrysts I) formed in a reaction between orthopyroxene and melt (Fig. 16a), while olivine with bladed to dendritic rims (their olivine phenocrysts II) has been interpreted to have formed in a reaction between olivine xenocrysts and host melt. The textures they describe strikingly resemble those of secondary olivine formed in our and previous experiments, and they also closely compare to textures of olivine phenocrysts that have been interpreted as primary magmatic (Fig. 16).

Boudier (1991) and Arndt *et al.* (2010) have interpreted subhedral to euhedral, commonly strain-free olivine “tablets” to have formed by recrystallization of deformed dunitic xenoliths and/or deformed olivine xenocrysts. An important point to note is that the olivine “tablets” they describe form single crystals with random orientations, while experimentally recrystallized olivine forms single crystals with dendritic branches. We consider it possible that the recrystallization of large, strongly deformed olivine xenocrysts as those described in the two studies may have resulted in the formation of randomly oriented,

single olivine grains. However, it also seems possible that the natural olivine crystals formed by peritectic reaction instead of recrystallization (i.e. that they largely replaced orthopyroxene or clinopyroxene that were originally intergrown with the deformed olivine crystals).

Natural olivine crystals with textures that, in our opinion, also closely compare to those of secondary olivine formed in melting experiments and to those of secondary olivine described by Ninomiya & Arai (1998) (Fig. 16a), have been described as primary magmatic from Kilauea volcano on Hawaii (e.g., Helz, 1987; Schwindinger & Anderson, 1989; Garcia, 1996; Vinet & Higgins, 2010), Piton de la Fournaise volcano on La Réunion (Albarède & Tamagnan, 1988; Welsch *et al.*, 2013), and several other locations worldwide (e.g., Larsen & Pedersen, 2000; Natland, 2003; Roedder *et al.*, 2006) (Fig. 16b-g). We do not attempt to evaluate the origin of olivine phenocrysts from the mentioned examples, but we would like to highlight their striking textural similarity with secondary olivine formed in melting experiments (Fig. 1 and Fig. 16) and urge that future studies consider primary as well as secondary origins for their formation. Except for their significantly larger size and tendency to show euhedral rather than subhedral-euhedral branches, olivine described as skeletal to dendritic compares to recrystallized olivine (Fig. 16b,d,f), while clusters of randomly oriented, euhedral to subhedral crystals compare to experimentally produced peritectic crystal cluster (Fig. 16c,e,g). The size difference may reflect kinetic controls and/or differences in crystallization time, while the euhedral character may reflect continued crystallization and/or ripening during prolonged magma residence. The close spatial association of the two olivine types is easily reconciled with a secondary origin, while mafic cumulates that may have been recycled to form the secondary olivine types are also known from most locations (e.g., Rançon *et al.*, 1989; Garcia, 1996; Upton *et al.*, 2000; Helz, 2009).

CONCLUSIONS

Primary as well as secondary magmatic growth produces dendritic to polyhedral olivine in experiments with textures that closely compare to each other. We suggest that (i) the shape and orientation of dendritic olivine crystals and their branches and (ii) the cluster shape and crystal distribution in clusters may be the best guides to distinguish recrystallized and peritectic olivine from primary magmatic crystals. Comparing textures of the experimental crystals with those of olivine from natural samples, we propose that dendritic phenocrysts and clusters of polyhedral crystals that are common in mafic igneous rocks worldwide should be evaluated for primary and potential secondary origins. Typical zoning patterns of recrystallized and peritectic olivine crystals or sub-microscopic textures remain unconstrained, but we suspect that they may reveal additional criteria to distinguish olivine of primary versus secondary origins. The effects of parameters such as temperature, magmatic H₂O contents, and crystallization times on olivine textures need further detailed investigation in experiments and through numerical modelling.

FUNDING

The experimental work carried out by S.E. was supported by a postdoctoral fellowship of the “Deutscher Akademische Austauschdienst” (DAAD, German Academic Exchange Service). We would also like to thank the Dalhousie University Electron Microprobe facility for generous access.

ACKNOWLEDGEMENTS

We greatly appreciate the detailed and constructive reviews by Benoit Welsch, Thomas Müller, and Nick Arndt which have helped us significantly to improve the presentation of our findings. We would like to thank Rémi Champallier, Philippe Teulat, and Didier Bellenoue for support with the experiments and Mike Dungan for sharing samples from the Tatara-San Pedro complex.

REFERENCES

- Albarède, F. & Tamagnan, V. (1988). Modelling the recent geochemical evolution of the Piton de la Fournaise volcano, Réunion Island, 1931-1986. *Journal of Petrology* **29**, 997-1030.
- Amma-Miyasaka, M. & Nakagawa, M. (2002). Origin of anorthite and olivine megacrysts in island-arc tholeiites: Petrological study of 1940 and 1962 ejecta from Miyake-Jima volcano, Izu-Mariana arc. *Journal of Volcanology and Geothermal Research* **117**, 263-283.
- Arndt, N. T., Guitreau, M., Boullier, A. M., Le Roex, A., Tommasi, A., Cordier, P. & Sobolev, A. (2010). Olivine, and the origin of kimberlite. *Journal of Petrology* **51**, 573-602.
- Boudier, F. (1991). Olivine xenocrysts in picritic magmas. *Contributions to Mineralogy and Petrology* **109**, 114-123.
- Brearley, M. & Scarfe, C. M. (1986). Dissolution rates of upper mantle minerals in an alkali basalt melt at high pressure: An experimental study and implications for ultramafic xenolith survival. *Journal of Petrology* **27**, 1137-1182.
- Clague, D. A. & Denlinger, R. P. (1994). Role of olivine cumulates in destabilizing the flanks of Hawaiian Volcanoes. *Bulletin of Volcanology* **56**, 425-434.
- Costa, F. & Dungan, M. (2005). Short time scales of magmatic assimilation from diffusion modeling of multiple elements in olivine. *Geology* **33**, 837-840.
- Costa, F., Dungan, M. & Singer, B. (2002). Hornblende- and phlogopite-bearing gabbroic xenoliths from Volcan San Pedro (36°S), Chilean Andes: Evidence for melt and fluid migration and reactions in subduction-related plutons. *Journal of Petrology* **43**, 219-241.

- Deer, W. A., Howie, R. A. & Zussman, J. (1966). An introduction to the rock forming minerals. Longman Group Limited: England.
- Di Carlo, I., Pichavant, M., Rotolo, S., Scaillet, B., (2006). Experimental crystallization of high-K arc basalts: the golden pumice, Stromboli volcano (Italy). *Journal of Petrology* **47**, 1317–1343
- Donaldson, C. H. (1974). Olivine crystal types in harrisitic rocks of the Rhum pluton and Archean spinifex rocks. *Geological Society of America Bulletin* **85**, 1721-1726.
- Donaldson, C. H. (1976). An experimental investigation of olivine morphology. *Contributions to Mineralogy and Petrology* **57**, 187-213.
- Donaldson, C. H. (1985). The rates of dissolution of olivine, plagioclase, and quartz in a basalt melt. *Mineralogical Magazine* **49**, 683-689.
- Dungan, M. & Davidson, J. (2004). Partial assimilative recycling of the mafic plutonic roots of arc volcanoes: An example from the Chilean Andes. *Geology* **32**, 773–776.
- Dungan, M. A., Wulff, A. & Thompson, R. (2001). Eruptive stratigraphy of the Tatara–San Pedro complex, 36°S, Southern volcanic zone, Chilean Andes: Reconstruction method and implications for magma evolution at longlived arc volcanic centers. *Journal of Petrology* **42**, 555–626.
- Dunworth, E.A. & Wilson, M. (1998). Olivine melilitites of the SW German Tertiary Volcanic Province: Mineralogy and petrogenesis. *Journal of Petrology* **39**, 1805-1836.
- Erdmann, S., Scaillet, B. & Kellett, D. A. (2010). Xenocryst assimilation and formation of peritectic crystal clusters during magma contamination: an experimental study. *Journal of Volcanology and Geothermal Research* **198**, 355-367.

- Erdmann, S., Scaillet, B. & Kellett, D. A. (2012). Textures of peritectic crystals as guides to reactive minerals in magmatic systems: new insights from melting experiments. *Journal of Petrology* **53**, 2231-2258.
- Famin, V., Welsch, B., Okumura, S., Bachèlery, P. & Nakashima, S. (2009). Three differentiation stages of a single magma at Piton de la Fournaise (Reunion hotspot). *Geochemistry, Geophysics, Geosystems* **10**, Q01007, doi:10.1029/2008GC002015.
- Faure, F., Arndt, N. & Libourel, G. (2006). Formation of spinifex texture in komatiites: An experimental study. *Journal of Petrology* **47**, 1591-1610.
- Faure, F. & Schiano, P. (2005). Experimental investigation of equilibration conditions during forsterite growth and melt inclusion formation. *Earth and Planetary Science Letters* **236**, 882-898.
- Faure, F., Schiano, P., Troliard, G., Nicollet, C. & Soulestin, B. (2007). Textural evolution of polyhedral olivine experiencing rapid cooling rates. *Contributions to Mineralogy and Petrology* **153**, 405-416.
- Garcia, M. O. (1996) Petrography and olivine and glass chemistry of lavas from the Hawaii Scientific Drilling Project. *Journal of Geophysical Research* **101**, 11,701-11,713.
- Helz, R.T. (1987). Diverse olivine types in lava of the 1959 eruption of Kilauea volcano and their bearing on eruption dynamics. *US Geological Survey Professional Papers* **1350**, 691-722.
- Helz, R. T. (2009). Processes active in mafic magma chambers: The example of Kilauea Iki Lava Lake, Hawaii. *Lithos* **111**, 37-46.
- Henderson, P., Sélo, M. & Storzer, D. (1986). An investigation of olivine crystal growth in a picrite dyke, using the fission track method. *Mineralogical Magazine* **50**, 27-31.
- Jacobs, D. A. B. (2012) Orthopyroxene stability within kimberlite magma: an experimental investigation. M. Sc. Thesis, University of Stellenbosch, 56 p.

- Jerram, D. A., Cheadle, M. C. & Philpotts, A. R. (2003). Quantifying the building blocks of igneous rocks: are clustered crystal frameworks the foundation? *Journal of Petrology* **44**, 2033–2051.
- Johannes, W., Koepke, J. & Behrens, H. (1994). Partial melting reactions of plagioclase and plagioclase-bearing systems. In: Parsons, I. (ed.) *Feldspars and their Reactions*. Dordrecht: Kluwer, pp. 161-194.
- Larsen, L. M. & Pedersen, A. K. (2000). Processes in high-Mg, high-T magmas: Evidence from olivine, chromite and glass in Palaeogene picrites from West Greenland. *Journal of Petrology* **41**, 1071-1098.
- Lofgren, G. (1989) Dynamic crystallization of chondrule melts of porphyritic olivine composition: Textures experimental and natural. *Geochimica et Cosmochimica Acta* **53**, 461-470.
- Maaløe, S., Hansen, B. (1982). Olivine phenocrysts of Hawaiian olivine tholeiite and oceanite. *Contributions to Mineralogy and Petrology* **81**, 203-211.
- Mattioli, M., Renzulli, A., Menna, M. & Holm, P. M. (2006). Rapid ascent and contamination of magmas through the thick crust of the CVZ (Andes, Ollagüe region): Evidence from a nearly aphyric high-K andesite with skeletal olivines. *Journal of Volcanology and Geothermal Research* **158**, 87-105.
- Moore, A. E. & Erlank, A. J. (1979). Unusual olivine zoning: evidence for complex physico-chemical changes during the evolution of olivine melilitite and kimberlite magmas. *Contributions to Mineralogy and Petrology* **70**, 391-405.
- Morgan, D. J. & Jerram, D. A. (2006). On estimating crystal shape for crystal size distribution analysis. *Journal of Volcanology and Geothermal Research* **154**, 1–7

- Natland, J. H. (2003). Capture of helium and other volatiles during the growth of olivine phenocrysts in picritic basalts from the Juan Fernandez Islands. *Journal of Petrology* **44**, 421-456.
- Ninomiya, A. & Arai, S. (1998). Polygenetic olivine phenocrysts in Okete basanite, New Zealand. *Journal of Mineralogy, Petrology, and Economic Geology* **93**, 235-249.
- O'Driscoll, B., Donaldson, C. H., Troll, V. R., Jerram, D. A. & Emeleus, C. H. (2007). An origin for harrisitic and granular olivine in the Rum Layered Suite, NW Scotland: a crystal size distribution study. *Journal of Petrology* **48**, 253-270.
- Pownceby, M. I. & O'Neill, H. St. C. (1994). Thermodynamic data from redox reactions at high temperatures. III. Activity-composition relations in Ni-Pd alloys from EMF measurements at 850-1250 K, and calibration of the NiO + Ni-Pd assemblage as a redox sensor. *Contributions to Mineralogy and Petrology* **116**, 327-339.
- Qian, Q. & Hermann, J. (2010). Formation of high-Mg diorites through assimilation of peridotite by monzodiorite magma at crustal depths. *Journal of Petrology* **51**, 1381-1416.
- Rançon, J.-P., Lerebour, P. & Augé, T. (1989). The Grand Brûlé exploration drilling: new data on the deep framework of the Piton de la Fournaise volcano. Part 1: Lithostratigraphic units and volcanostructural interpretation. *Journal of Volcanology and Geothermal Research* **36**, 113-127.
- Roeder, P. L., Gofton, E. & Thornber, C. (2006). Cotectic proportions of olivine and spinel in olivine-tholeiitic basalt and evaluation of pre-eruptive processes. *Journal of Petrology* **47**, 883-900.
- Scaillet, B., Pichavant, M. & Roux, J. (1995). Experimental crystallization of leucogranite magmas. *Journal of Petrology* **36**, 663-705.

- Scaillet, B. & Evans, B. (1999). The 15 June 1991 eruption of Mount Pinatubo. I. Phase equilibria and pre-eruption P–T– $f_{\text{H}_2\text{O}}$ – f_{O_2} conditions of the dacite magma. *Journal of Petrology* **40**, 381-411.
- Schwindinger, K. R. & Anderson, A. T. (1989). Synneusis of Kilauea Iki olivines. *Contributions to Mineralogy and Petrology* **103**, 187-198.
- Shea, T. & Hammer, J. E. (2013). Kinetics of cooling- and decompression-induced crystallization in hydrous mafic-intermediate magmas. *Journal of Volcanology and Geothermal Research* **260**, 127-145.
- Streck, M. J. (2008). Mineral textures and zoning as evidence for open system processes. *Reviews in Mineralogy & Geochemistry* **69**, 595-622.
- Sunagawa, I. (2005). Crystals: growth, morphology and perfection. Cambridge University Press: Cambridge. 295 p.
- Thornber, C. R. & Huebner, J. S. (1985). Dissolution of olivine in basaltic liquids: experimental observations and applications. *American Mineralogist* **70**, 934-945.
- Tröger, W. E. (1952). Optische Bestimmung der gesteinsbildenden Minerale. E. Schweizerbart'sche Verlagsbuchhandlung (Nägele und Obermiller): Stuttgart.
- Tsuchiyama, A. (1985). Dissolution kinetics of plagioclase in the melt of the system diopside-albite-anorthite, and origin of dusty plagioclase in andesites. *Contributions to Mineralogy and Petrology* **89**, 1-16.
- Tsuchiyama, A. (1986). Experimental study of olivine-melt reaction and its petrological implications. *Journal of Volcanology and Geothermal Research* **29**, 245-264.
- Upton, B. G. J., Semet, M. P. & Joron, J. L. (2000). Cumulate clasts in the Bellecombe Ash Member, Piton de la Fournaise, Réunion Island, and their bearing on cumulative

processes in the petrogenesis of the Réunion lavas. *Journal of Volcanology and Geothermal Research* **104**, 297-318

Vinet, N. & Higgins, M. D. (2010). Magma solidification processes beneath Kilauea Volcano, Hawaii: a quantitative textural and geochemical study of the 1969-1974 Mauna Ulu lavas. *Journal of Petrology* **51**, 1297-1332.

Welsch, B., Faure, F., Famin, V., Baronnet, A. & Bachèlery, P. (2013). Dendritic crystallization: a single process for all the textures of olivine in basalts? *Journal of Petrology* **54**, 539-574.

Whitney, D. L. & Evans, B. W. (2010). Abbreviations for names of rock-forming minerals. *American Mineralogist* **95**, 185–187.

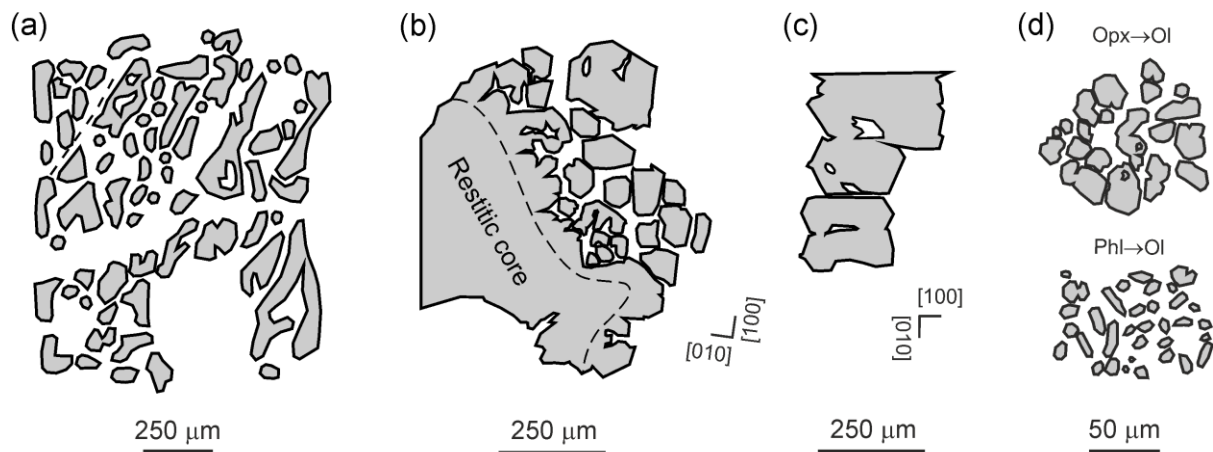
FIGURE CAPTIONS:

Figure 1 - Erdmann et al.

Figure 1: Line drawings of recrystallized olivine and peritectic olivine produced by experimental partial melting. Drawings after microphotographs of (a) recrystallized (“vermicular”) olivine of Tsuchiyama (1986) (his Figs 2h and 5); (b,c) recrystallized (“euhedral”) olivine of Boudier (1991) (her Fig. 2a,b); and (d) two peritectic olivine clusters formed after orthopyroxene (Opx) and phlogopite (Phl) of Erdmann *et al.* (2012) (their Fig. 4 a,d). Recrystallized olivine is characterized by euhedral to subhedral branches; peritectic olivine forms cluster of randomly oriented crystals.

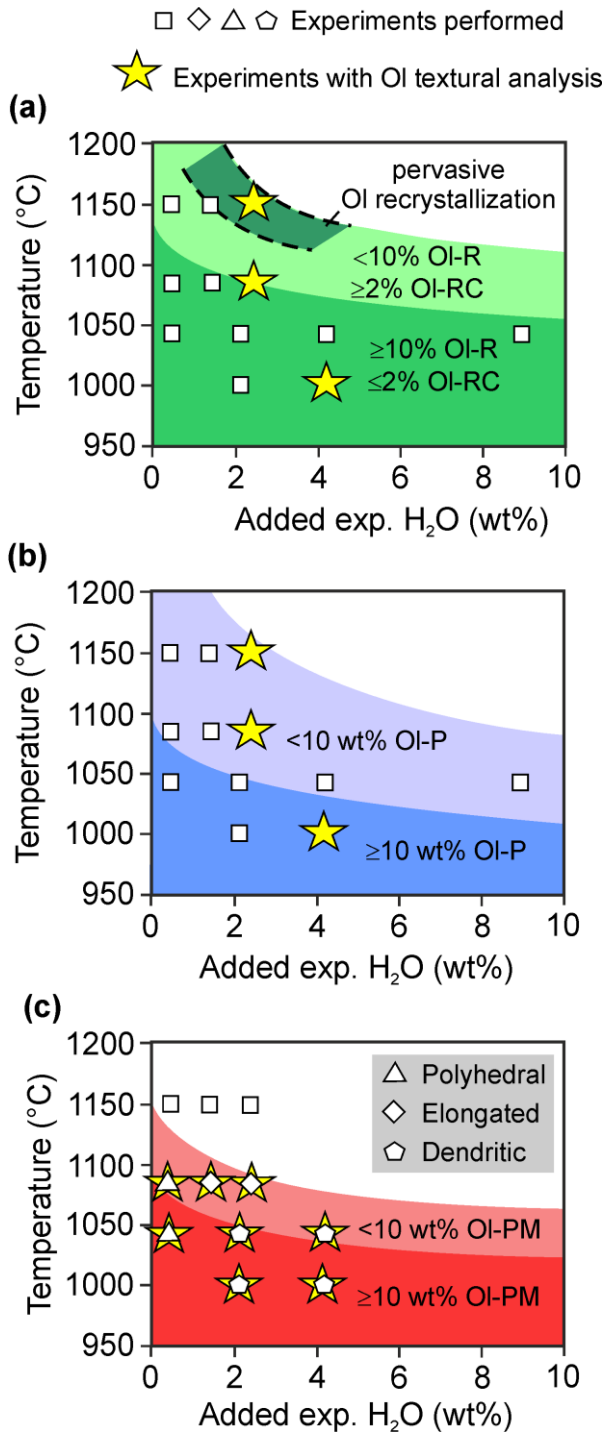


Figure 2 - Erdmann et al.

Figure 2: Summary of olivine occurrence and abundance (a,b) in melting experiments shown for the melanorite (MN) starting material; and (c) in basalt (B) crystallization experiments. (a) In the MN melting experiments, restitic (Ol-R), partially to largely recrystallized olivine (Ol-RC), and peritectic olivine are present in all experiments performed. (b) Olivine also

formed in all ≤ 1085 °C B crystallization experiments, ranging in shape from polyhedral over elongated to dendritic. The complete assemblages of the experimental run products are reported in Table 1.

Olivine		Main characteristics of olivine in melting experiments
OI-R		Restitic olivine: Angular to rounded, normally or reversely zoned, locally with healed micro fractures and abundant nano pores
OI-RC		Recrystallized olivine (with irregular restitic core): Recrystallized OI has subhedral to euhedral protrusions or branches with short prismatic habit, largely unzoned
OI-P-Opx ^a		Peritectic OI formed after Opx: Cluster of randomly oriented, subhedral-euhedral, relatively large, and short prismatic crystals, largely unzoned
OI-P-Amp ^b		Peritectic OI formed after Amp: Cluster of randomly oriented, subhedral-euhedral, relatively small, and short prismatic crystals, largely unzoned
OI-P-Phl ^c		Peritectic OI formed after Phl: Cluster of randomly oriented, subhedral-euhedral, relatively small, and acicular crystals, largely unzoned

Figure 3 - Erdmann et al.

Figure 3: Summary of olivine subtypes present in our melting experiments. a, b, c = olivine types OI2b, OI2c, and OI2d of Erdmann *et al.* (2012). Opx=orthopyroxene; Amp=amphibole; Phl=phlogopite.

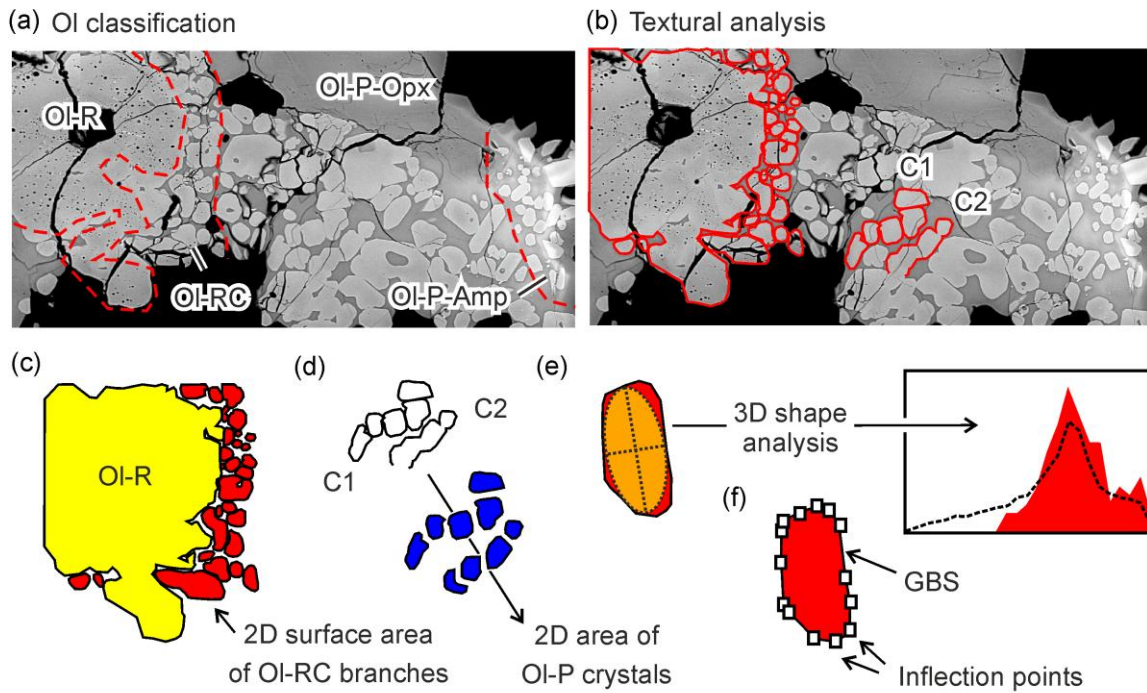


Figure 4 - Erdmann et al.

Figure 4: Example of (a) olivine classification (b-e) and textural analysis. (b-d) Olivine branches and peritectic crystals were manually outlined. (d) For clusters of touching peritectic crystals, individual crystals were distinguished using transmitted light microscopy. (c,d) The 2D surface area of each branch/crystal was then determined using the SCION image software. (e) The major and minor axes of the best-fitting ellipse of olivine branches and peritectic crystals and the CSDslice program of Morgan & Jerram (2006) were used to calculate 3D shapes. (f) The length of euhedral grain boundary segments (GBSs) was measured between inflection points.

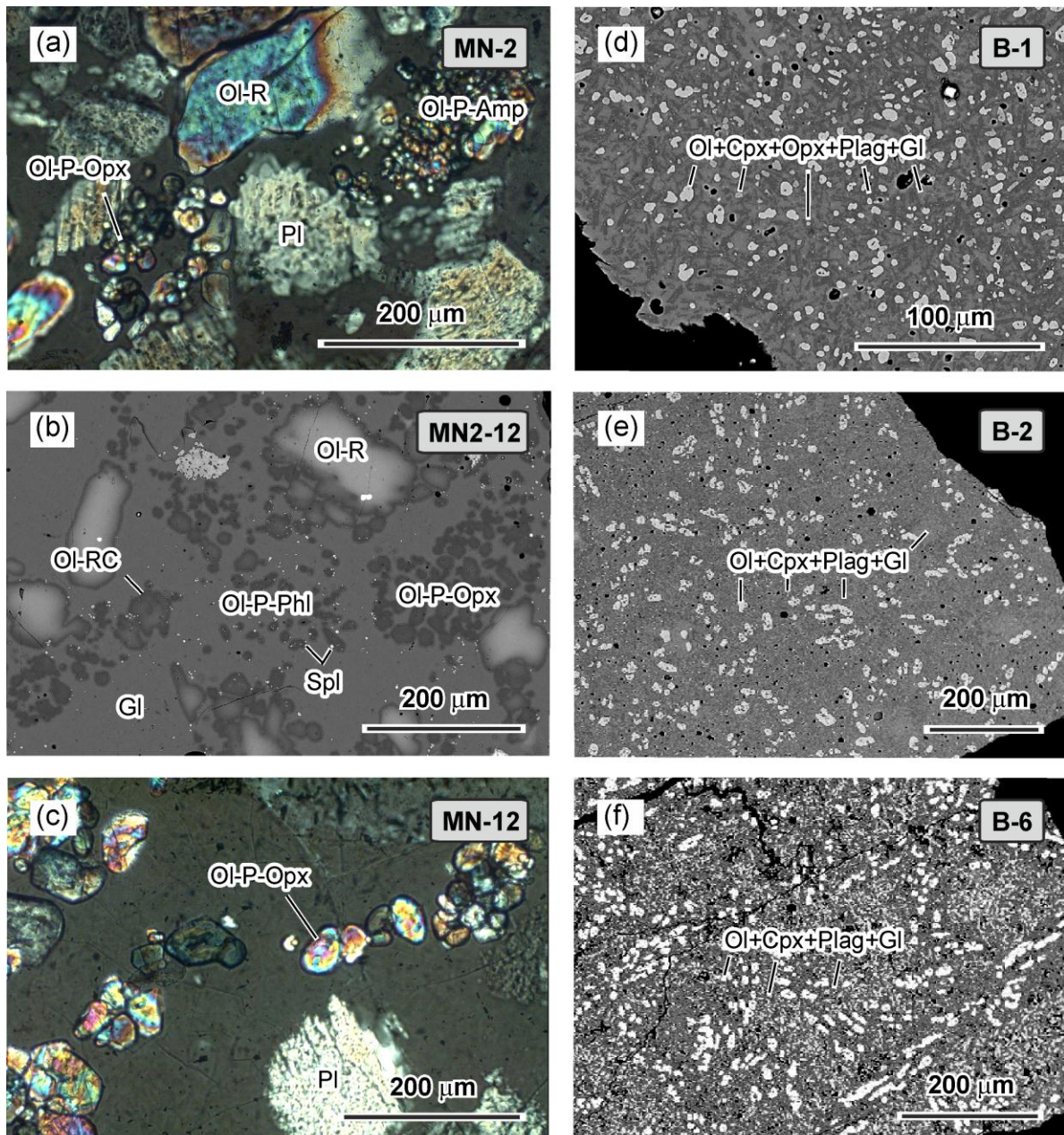


Figure 5 - Erdmann et al.

Figure 5: Microphotographs and BSE images showing typical phase distributions and the textures of the assemblages for (a-c) melting experiments and (d-f) crystallization experiments. Textures of the melting experiments are more heterogeneous than those of the crystallization experiments, but significant concentration of crystals or preferred orientations have not been detected. (d-f) Olivine is the brightest phase. Other phases present are: (i)

clinopyroxene and orthopyroxene, <math><10\ \mu\text{m}</math> in maximum dimension, intermediate gray scales; (ii) plagioclase, darkest phase; and (iii) interstitial glass, intermediate to dark gray scale.

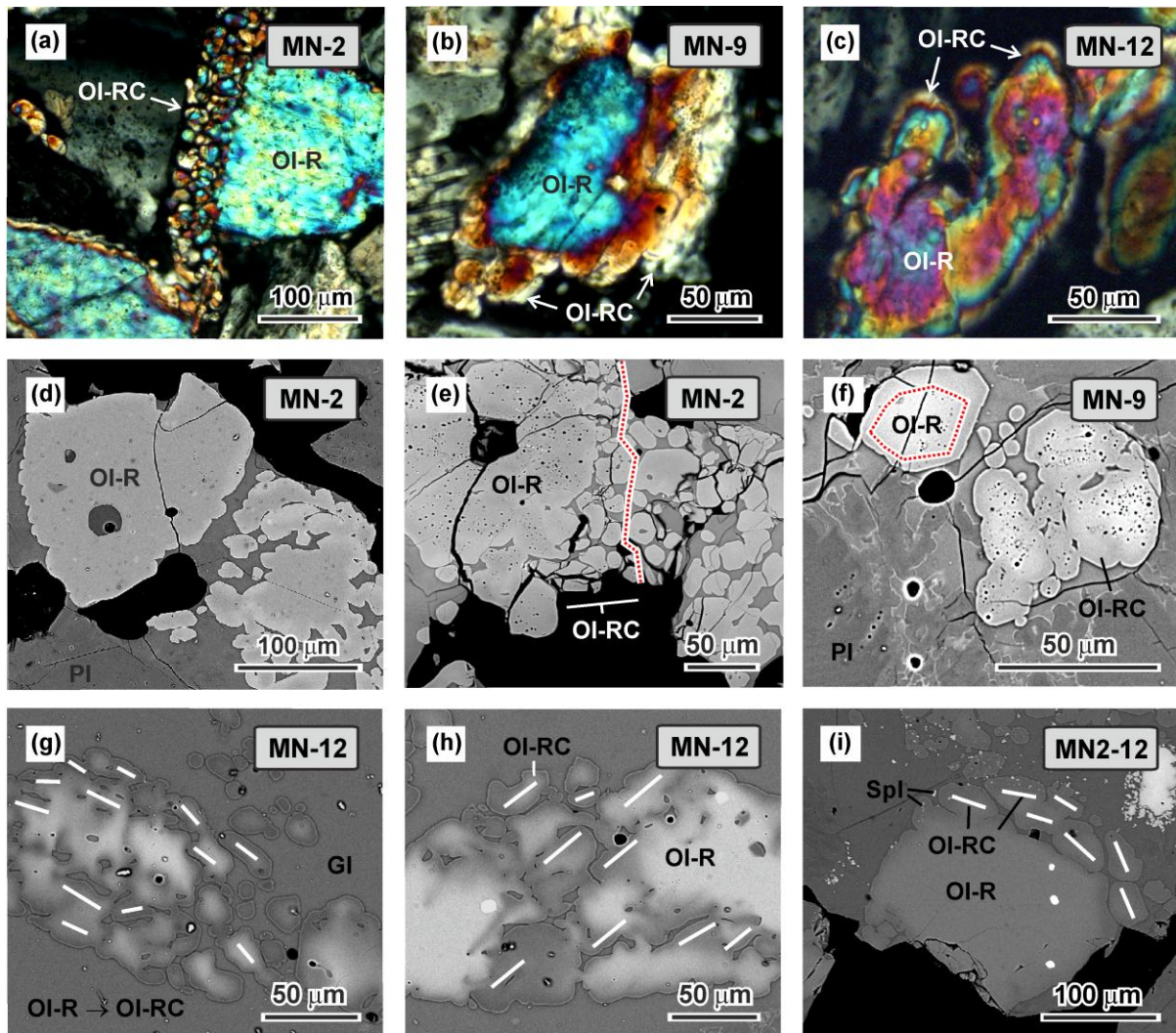


Figure 6 - Erdmann et al.

Figure 6: Transmitted light microphotographs and BSE images of recrystallized olivine in melting experiments. Gl = glass; OI-R = restitic olivine; OI-RC = recrystallized olivine; Spl = spinel. (a) Restitic olivine with a sharp recrystallized rim composed of branches in optical continuity. (b,c) Restitic olivine with recrystallized rims consisting of subhedral to euhedral, optically continuous branches. (d) Restitic olivine with regular embayments and some euhedral grain boundary segments. (e,f) Partially recrystallized olivine with abundant nanopores in restitic cores. (g,h) Restitic olivine with pervasive dissolution and partial

recrystallization along grain margins and melt channels. (i) Restitic olivine with marginal recrystallization. Euhedral spinel inclusions are common in the recrystallized zones.

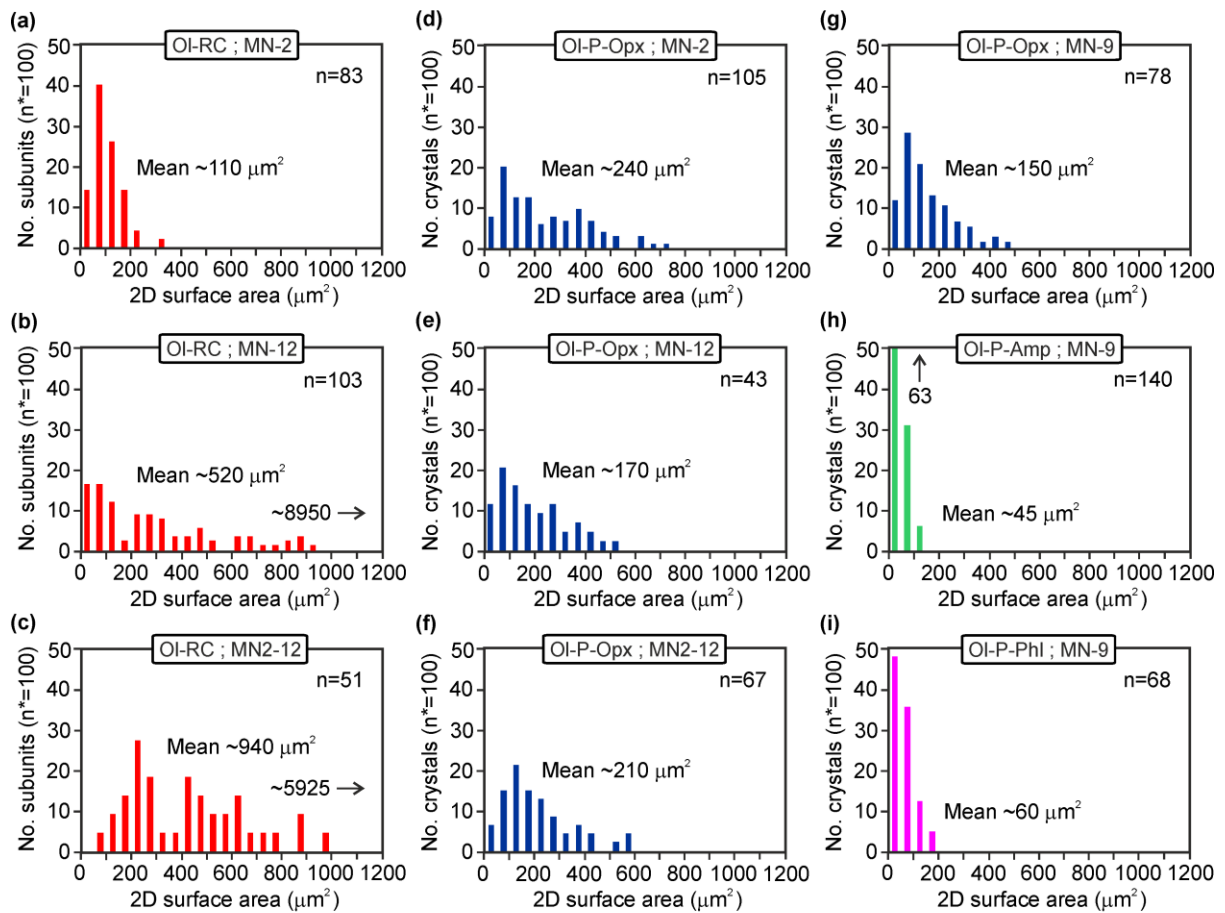


Figure 7 - Erdmann et al.

Figure 7: Summary of 2D surface area data for (a-c) branches of recrystallized olivine, and (d-i) peritectic olivine produced in melting experiments. Figures 7 b and c show part of the dataset; inset numbers indicate the complete range. The mean 2D surface area decreases from OI-RC formed in the high-temperature experiments MN-12 and MN2-12 (b,c) over peritectic crystals formed by orthopyroxene replacement (d-g) to those formed by phlogopite and amphibole replacement (h,i). n = number of analyses; n* = values normalized to 100.

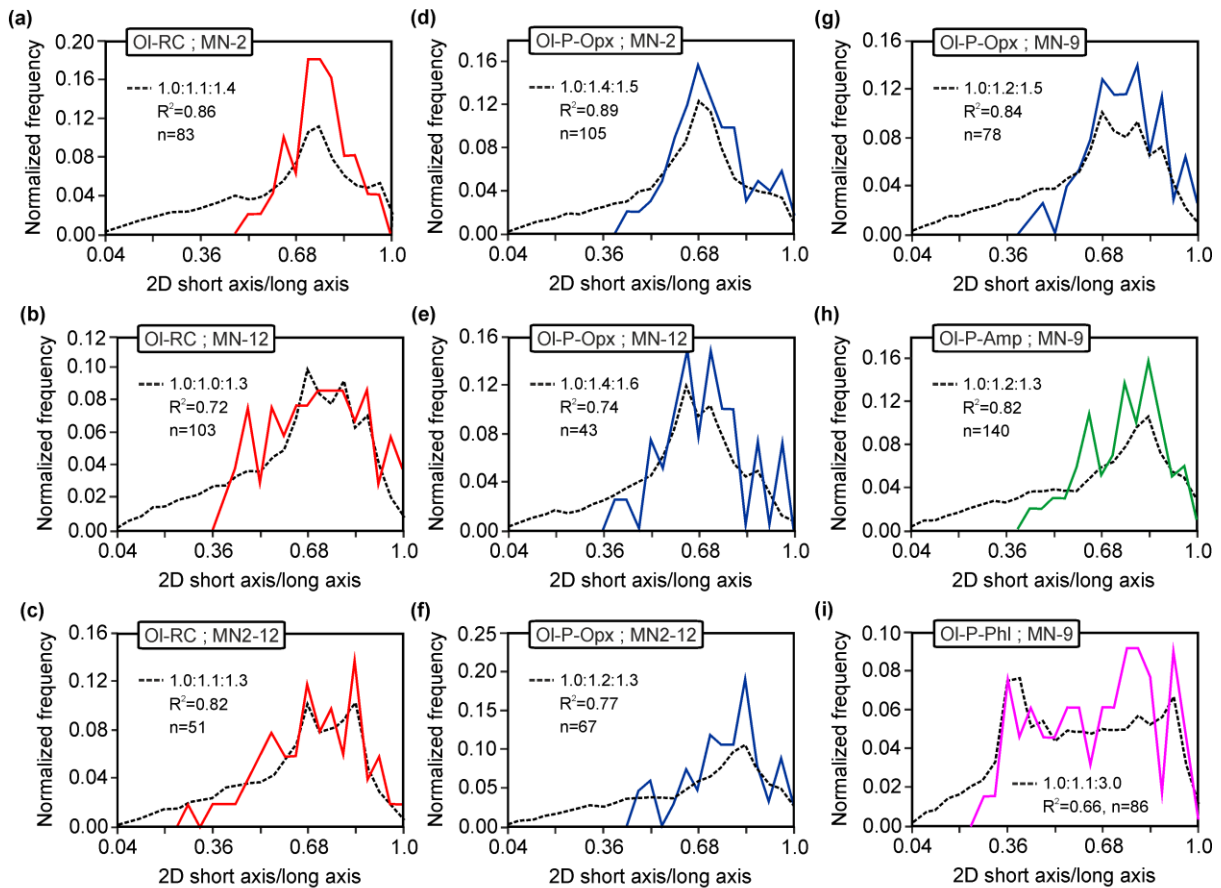


Figure 8 - Erdmann et al.

Figure 8: Summary of 3D shape analysis for (a-c) branches of recrystallized olivine, and (d-i) peritectic olivine produced in melting experiments. Recrystallized olivine branches (a-c) and peritectic crystals formed after orthopyroxene and amphibole (d-g) are short prismatic, while olivine replacing phlogopite is acicular (i). n = number of analyses; R^2 = calculated reliability of the shape estimate. For comparison, typical axial ratios of forsterite-rich, polyhedral olivine are $\sim 1.5:1:2$ for a-, b-, and c-axes (Tröger, 1952; Deer *et al.*, 1966), while elongated and dendritic crystals tend to have tabular shapes ($a > c \gg b$) (Donaldson, 1976).

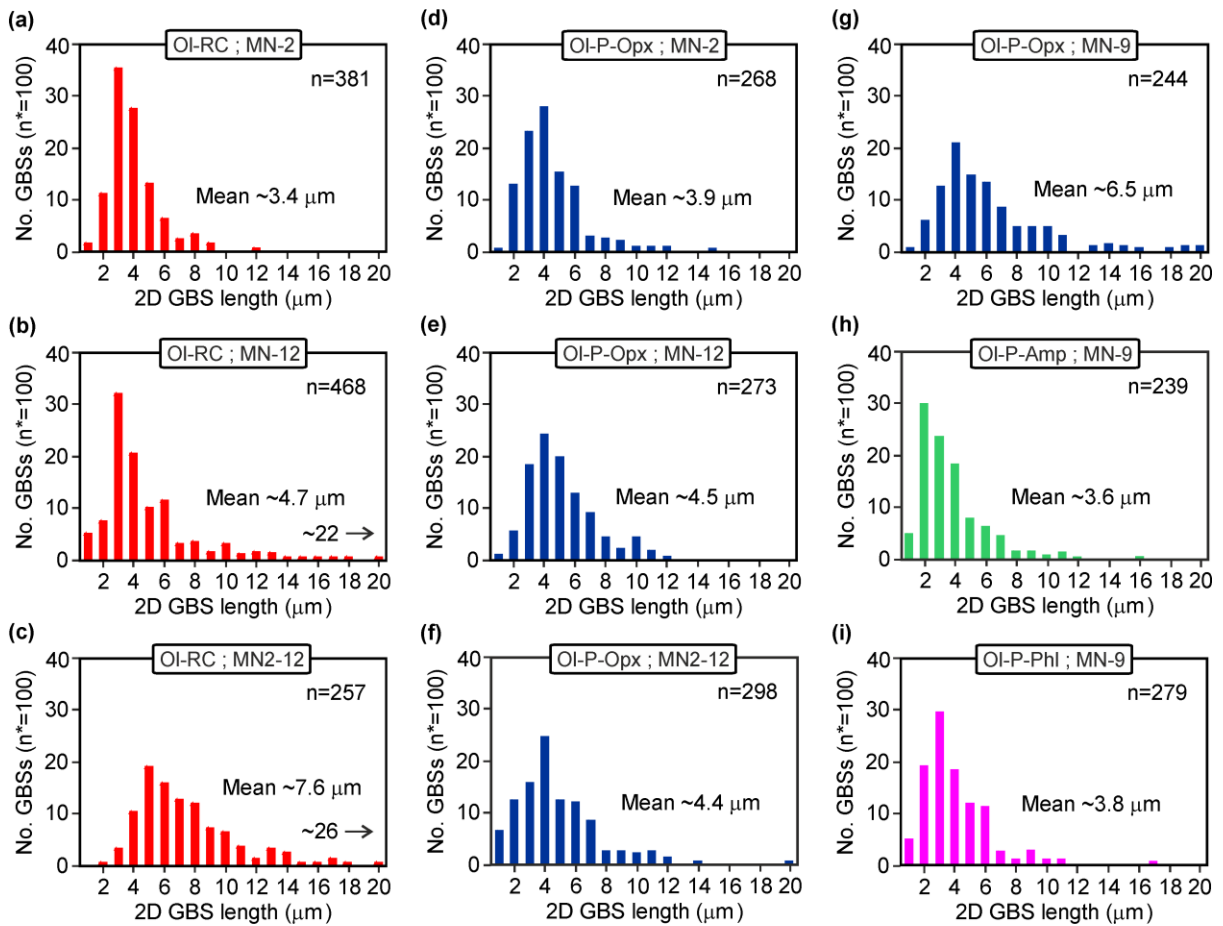


Figure 9 - Erdmann et al.

Figure 9: Summary of 2D GBS length patterns for (a-c) branches of recrystallized olivine, and (d-i) peritectic olivine produced in melting experiments. Figures 9 b and c show part of the dataset; inset numbers indicate the complete range. The mean 2D GBS length tends to decrease with experimental temperature; however, there is considerable scatter in the datasets (e.g., Fig. 9d versus Fig. 9e). Values are lowest for recrystallized olivine branches formed at low temperature and for olivine that replaced amphibole and phlogopite. n= number of analyses; n*= values normalized to 100.

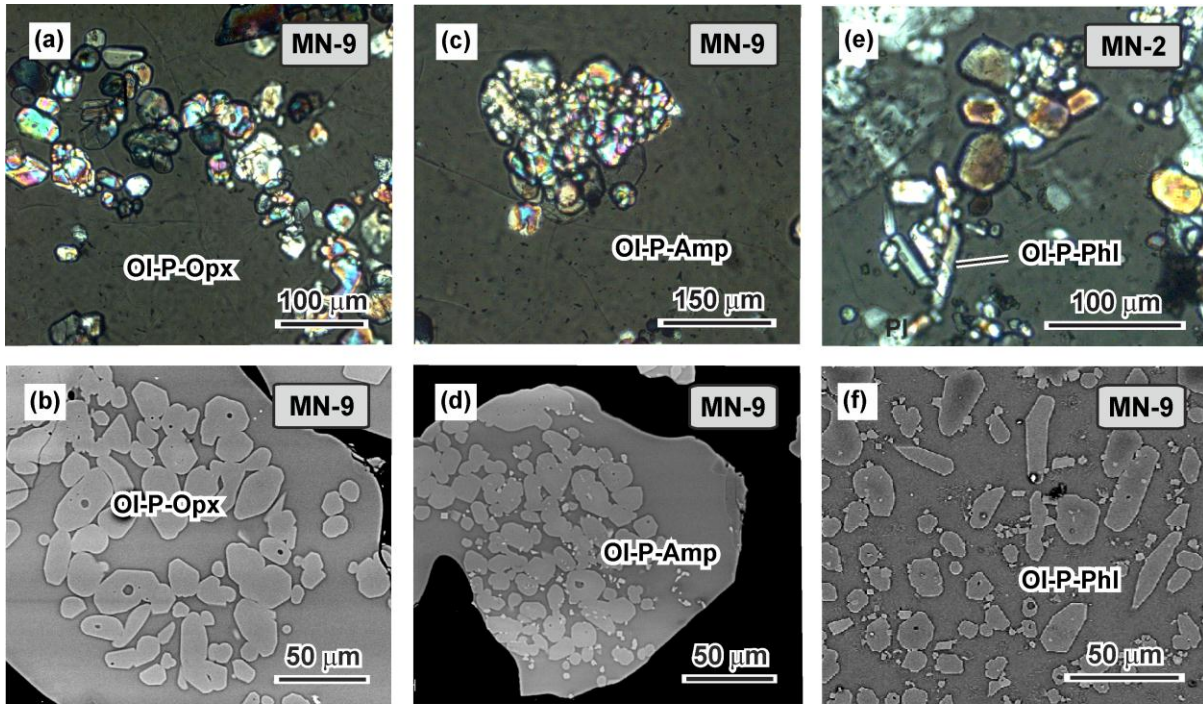


Figure 10 - Erdmann et al.

Figure 10: Transmitted light microphotographs (a,c,e) and BSE images (b,e,f) of peritectic olivine in melting experiments. (a) Peritectic olivine that replaced orthopyroxene forms relatively large crystals in loose clusters. (b) Olivine that replaced orthopyroxene formed relatively small crystals in dense clusters. (c) Olivine that replaced amphibole formed relatively small crystals in dense clusters. (d) Olivine crystallized after amphibole forms relatively small crystals in dense clusters. (e) Olivine crystallized after phlogopite forms relatively small crystals in loose clusters. (f) Olivine crystallized after phlogopite forms relatively small crystals in loose clusters.

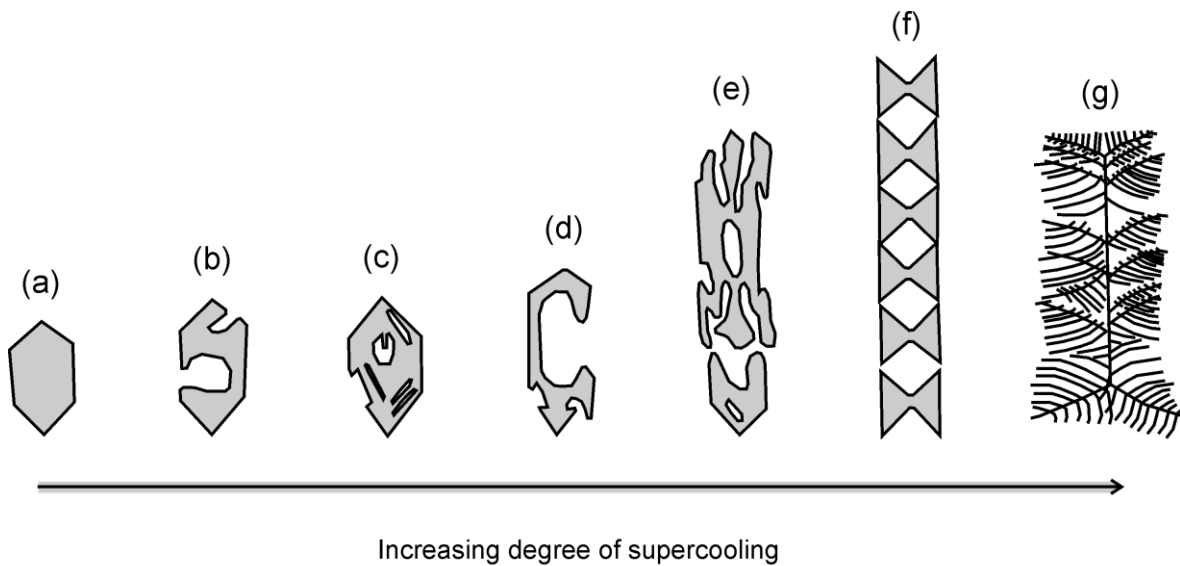


Figure 11 - Erdmann et al.

Figure 11: Line drawings of primary magmatic olivine formed in crystallization experiments of Donaldson (1976). The olivine crystals formed at variable degrees of supercooling, following supra-liquidus heating of the charges. (a) polyhedral, (b-d) skeletal to hopper-shaped, and (e-g) dendritic olivine. The shape of the dendritic olivine sketched in Fig. 11e closely compares to dendritic crystals formed in our experiments (Figs 12, 13).

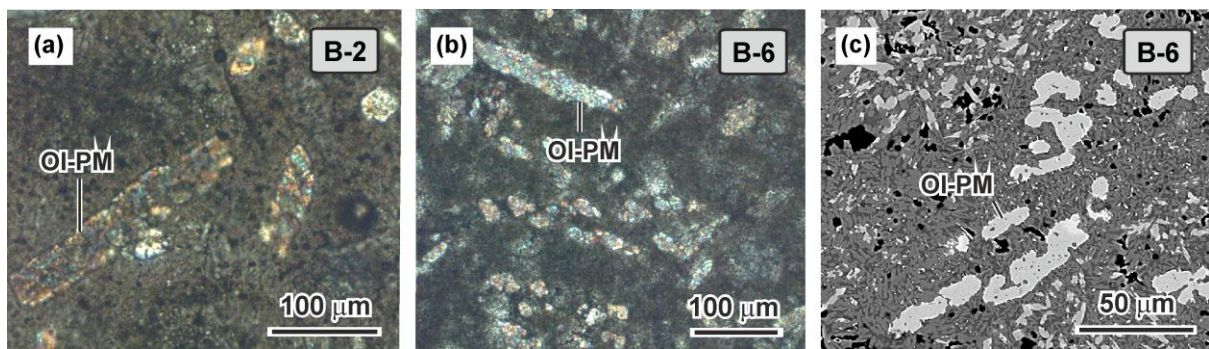


Figure 12 - Erdmann et al.

Figure 12: Transmitted light (a,b) and BSE images (c) of primary magmatic olivine dendrites in our basalt crystallization experiments. Crystals and their branches are elongated.

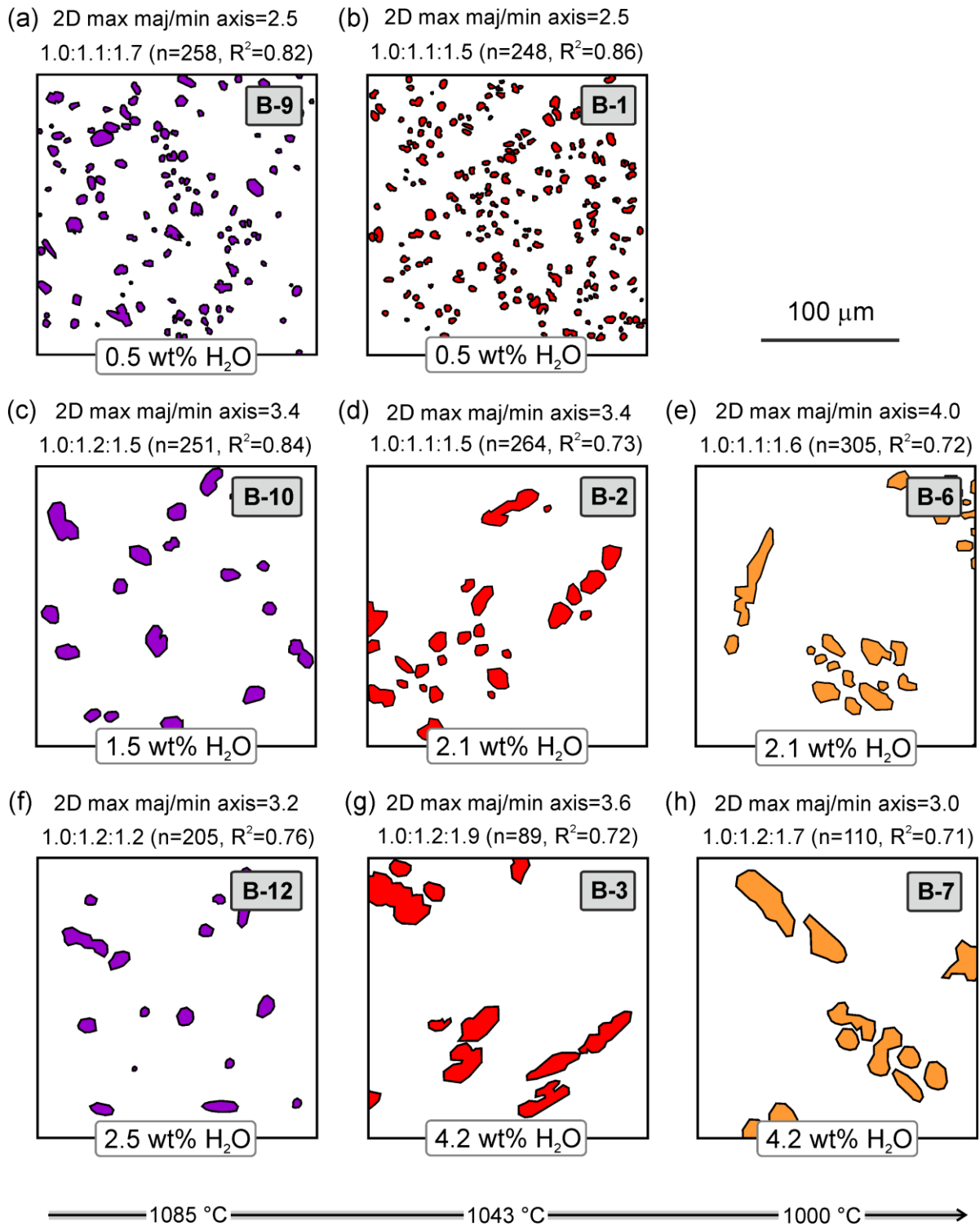


Figure 13 - Erdmann et al.

Figure 13: Representative line drawings and shape analysis of primary magmatic olivine formed in our basalt crystallization experiments. We note that the calculated 3D shape yields prismatic morphologies for olivine from all charges, while the reliability of the shape

estimate decreases from $R^2 \geq 0.82$ to ≤ 0.73 . Visual inspection and our 2D measurements indicate that polyhedral olivine formed in low- H_2O experiments (a,b), elongated olivine formed in high-temperature experiments with intermediate H_2O contents (c,f), and skeletal crystals formed at low temperatures and intermediate to high H_2O contents.

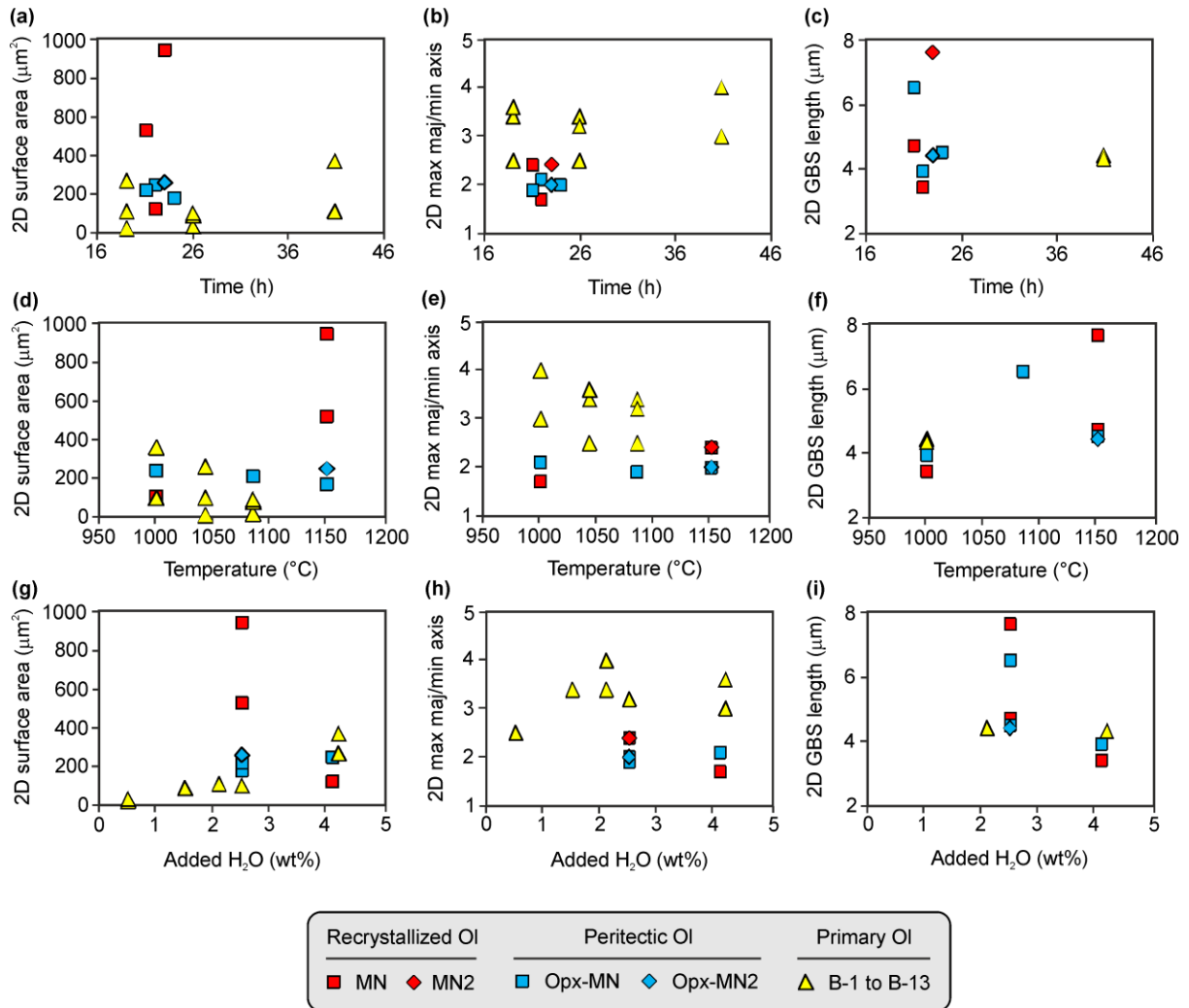


Figure 14 - Erdmann et al.

Figure 14: Variation of olivine textures with experimental (a-c) run time, (d-f) temperature, and (g-i) H_2O content for recrystallized olivine, peritectic olivine formed after orthopyroxene, and primary magmatic olivine. Shown are average values for crystal size, shape, and grain boundary segmentation. The average 2D surface area and 2D grain boundary segment (GBS) lengths are variably affected by experimental temperature and H_2O content (we note that GBS lengths were measured for only two crystallization experiments, B-6 and B-7). The

average 2D shape of olivine branches distinguishes recrystallized and primary magmatic olivine (b,e,h). The variation in run time has had no observable effect on the olivine textures.

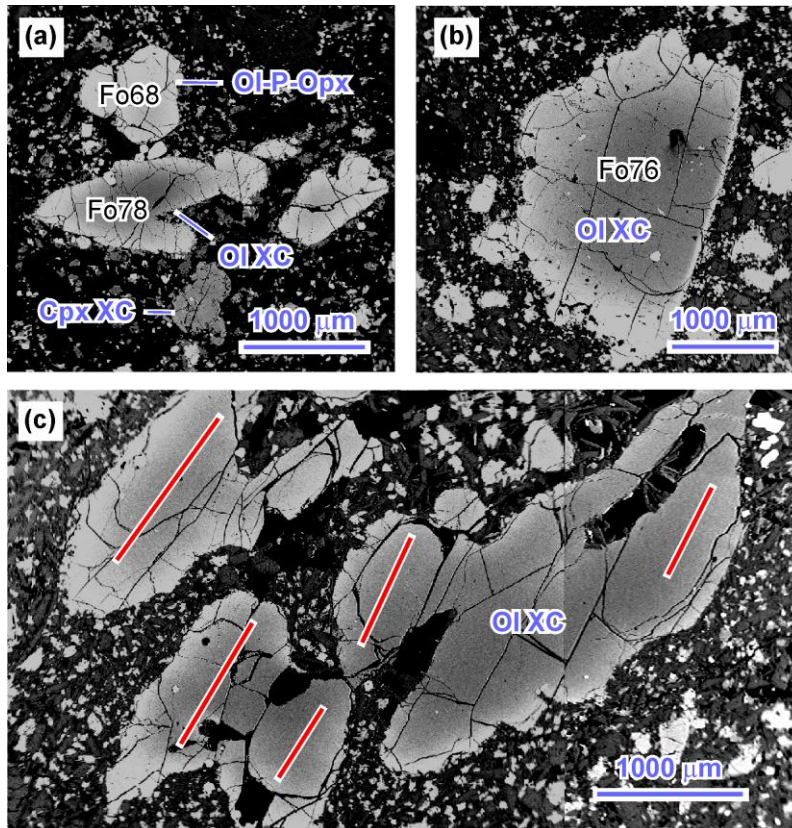


Figure 15 - Erdmann et al.

Figure 15: Olivine crystals in basaltic lavas of the Tataro-San Pedro volcanic complex, Chile. (a) Cluster of subhedral to euhedral, inclusion-poor olivine crystals are interpreted as peritectic olivine. Xenocrysts (XC) are commonly associated with these clusters. (b) Fragment of an olivine xenocryst. Xenocryst cores are commonly more Fo-rich than the inferred peritectic crystals. They also locally contain healed microfractures. Note that this xenocryst fractured shortly prior to eruption, shown by the sharp and thin Fo-poor rim along its fracture surface. (c) Dendritic olivine crystals are relatively rare. They are interpreted to have formed by dissolution and partial recrystallization.

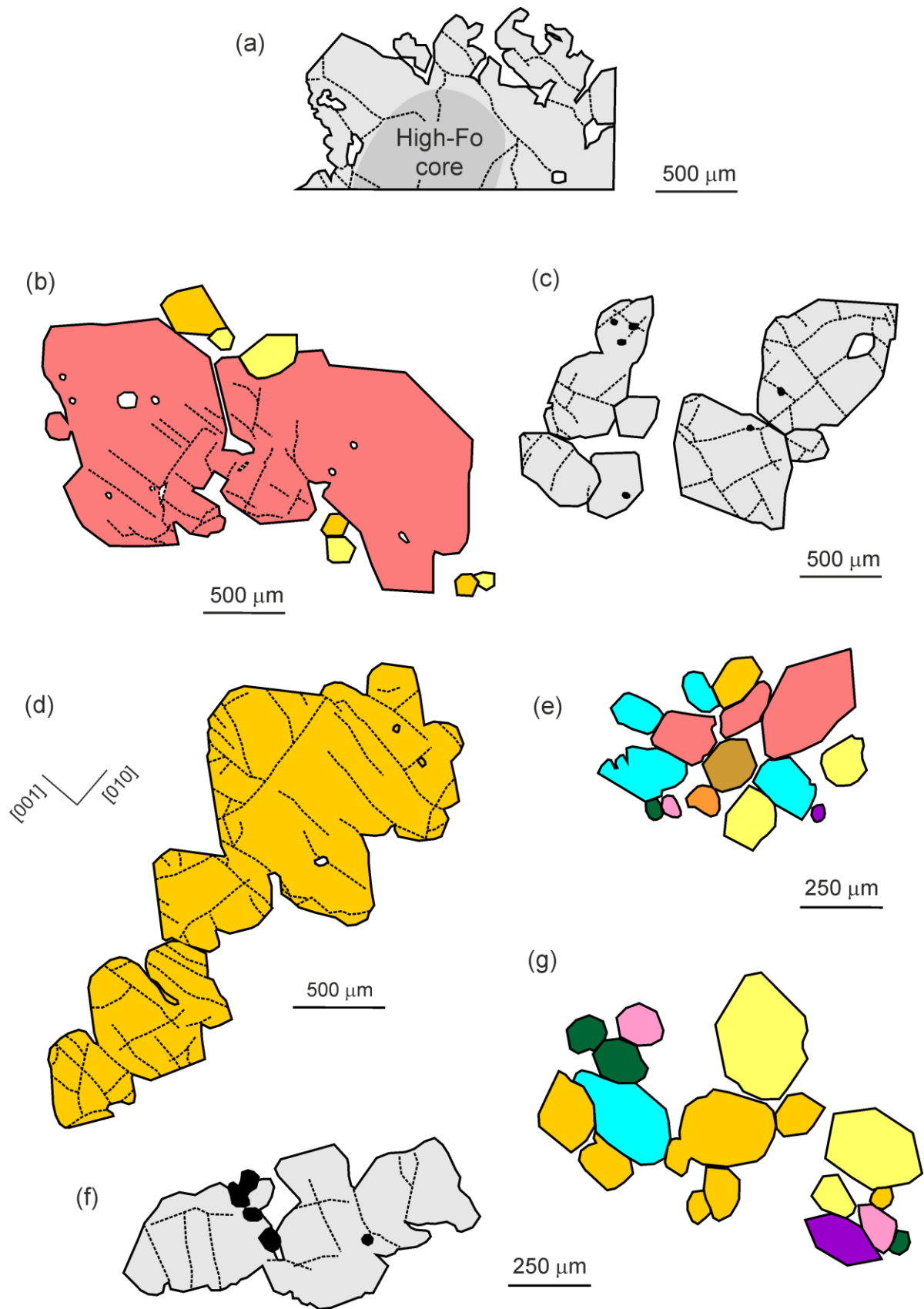


Figure 16 - Erdmann et al.

Figure 16: Line drawings of dendritic olivine and clusters of polyhedral olivine from literature examples. Olivine crystals shown have been interpreted as secondary magmatic (a) and primary magmatic (b-g). (a) Okete basanite, New Zealand (after Ninomiya & Arai, 1998), (b,c) Kilauea volcano on Hawaii (after Helz, 1987), (d,e) Piton de la Fournaise volcano on La Réunion (after Welsch *et al.*, 2013), and from (f,g) the Vaigat Formation in West Greenland (after Larsen & Pedersen, 2000). (a) Rim of an olivine phenocryst (I) of Ninomiya & Arai (1998) (their Fig. 4c); (b) skeletal olivine aggregate, Helz (1987) (her Fig. 25.6A,B); (c) cluster of euhedral “class 2” olivine, Helz 1987 (her Fig. 25.5C); (d) dendritic olivine, Welsch *et al.* (2013) (their Fig. 9c); (e) non-ordered groups of polyhedral olivine, Welsch *et al.* (2013) (their Fig. 13a); (f) cluster of olivine in optical continuity, Larsen & Pedersen (2000) (their Fig. 3b); and (g) loose cluster of clear euhedral olivine, Larsen & Pedersen (2000) (their Fig. 3b). Stippled lines indicate clearly visible fractures and cleavage planes. Different colours indicate variable optical orientation, but they do not correspond to interference colours of the original microphotographs. The cluster depicted in Fig. 16c also consists of randomly oriented crystals, but the image was redrawn from an un-polarized transmitted light microphotograph and the crystal orientations are therefore unknown.

Table 1: Experimental conditions and run products

Experiment	T	H ₂ O	t	ΔFeO	Phase proportions (wt%)									
	(°C)	(wt%)	(h)	%	Ol-PM	Ol-R	Ol-RC	Ol-P	Pl	Cpx	Opx	Amp	Spl	Gl
MN-2*	1000	4.1	22	n.a.	-	12	2	14	46	0	0	0	<1	17
MN-9*	1085	2.5	24	-23	-	7	2	8	31	-	-	-	<1	53
MN-12*	1150	2.5	21	-39	-	3	3	4	19	-	-	-	<1	71
MN2-12	1150	2.5	23	-24	-	12	8	25	-	-	-	-	2	53
B-6#	1000	2.1	41	n.a.	18	-	-	-	36	6	-	11	-	29
B-7	1000	4.2	41	n.a.	11	-	-	-	35	1	-	8	-	45
B-1#	1043	0.5	19	n.a.	11	-	-	-	34	7	2	-	-	46
B-2	1043	2.1	19	15	10	-	-	-	29	4	-	-	-	58
B-3	1043	4.2	19	10	5	-	-	-	12	-	-	-	-	83
B-9#	1085	0.5	26	n.a.	9	-	-	-	22	-	-	-	-	69
B-10	1085	1.5	26	-33	5	-	-	-	18	-	-	-	-	77
B-12	1085	2.5	26	-32	4	-	-	-	12	-	-	-	-	84

MN and MN2 = melanorite melting experiments; B = basalt crystallization experiment. * = Data from Erdmann *et al.* (2012). Phase assemblages of melting experiments were estimated by mass balance. Phase proportions estimated by point counting of BSE images. Experimental Fe loss (ΔFeO) was calculated as $100 \times (\text{FeO}_{\text{Charge}} - \text{FeO}_{\text{St.Mat.}}) / \text{FeO}_{\text{St.Mat.}}$, where $\text{FeO}_{\text{Charge}}$ is calculated from crystals and glass. Iron loss estimates for 1000 °C experiments are not available. Ol= all olivine of the charge; Ol-R=restitic olivine; Ol-RC=recrystallized olivine; Ol-P=peritectic olivine; and Ol-PM= primary magmatic olivine.

Table 2: Composition of whole-rock and glass starting materials normalized to 100 wt%

Material	SiO ₂	TiO ₂	Al ₂ O ₃	Fe ₂ O ₃	MnO	MgO	CaO	Na ₂ O	K ₂ O	P ₂ O ₅	Total
MN-wr [#]	45.95	0.44	22.42	7.02	0.11	10.79	10.62	2.12	0.46	0.07	**99.44
MN2-wr	42.66	0.27	9.79	15.78	0.22	25.39	4.83	0.78	0.23	0.06	**100.61
B-gl	50.91	0.95	19.43	9.23	0.17	6.23	9.27	*3.23	0.57	-	**99.24

MN, MN2 = two melanorite samples; B = basalt; wr = whole-rock and gl = glass starting materials. # Analysis from Erdmann et al. (2010). Total Fe given as Fe₂O₃. * Corrected relative to glass standards of Scaillet & Evans (1999). ** Pre-normalized analytical totals.

Table 3: Textural data for recrystallized, peritectic, and primary magmatic olivine produced in melting and crystallization experiments

Olivine type	<i>Recrystallized OI (OI-RC)</i>			<i>Peritectic OI (OI-P)</i>						<i>Primary magmatic olivine (OI-PM)</i>							
Olivine type	OI-RC	OI-RC	OI-RC	OI-P-Opx	OI-P-Opx	OI-P-Opx	OI-P-Opx	OI-P-Amp	OI-P-Phl	P	P	E	D	D	E	D	D
Experiment	MN-2	MN-12	MN2-12	MN-2	MN-12	MN2-12	MN-9	MN-9	MN-9	B-9	B-1	B-10	B-2	B-6	B-12	B-3	B-7
T (°C)	1000	1150	1150	1000	1150	1150	1085	1085	1085	1085	1043	1085	1043	1000	1085	1043	1000
2D surface area of OI branches (for OL-RC and OI-PM) and crystals (for OI-P) in μm^2																	
n	83	103	51	105	43	67	78	140	66	258	248	251	264	305	205	89	110
Mean	108	520	940	238	174	210	152	45	63	19	12	81	98	99	89	259	360
Maximum	337	8946	5924	770	518	595	494	129	195	100	36	391	543	844	498	1866	1767
σ	61	1058	1080	169	122	139	105	28	41	18	8	57	82	86	63	313	285
<i>d</i>	13	208	302	33	37	34	24	6	10	16	16	16	16	17	14	9	10
2D GBS length of OI branches and crystals in μm																	
n	381	468	257	268	273	298	244	339	279	-	-	-	-	420	-	-	262
Mean	3.4	4.7	7.6	3.9	4.5	4.4	6.5	3.6	3.8	-	-	-	-	4.4	-	-	4.3
Maximum	12	22	26	15	12	20	44	16	18	-	-	-	-	14	-	-	21
σ	1.6	3.2	3.6	2.0	2.2	2.6	5.3	1.9	2.0	-	-	-	-	2.3	-	-	3.3
<i>d</i>	0.2	0.3	0.4	0.2	0.3	0.3	0.7	0.2	0.2	-	-	-	-	0.2	-	-	0.4
3D and 2D shape estimates for OI branches (OI-RC and OI-PM) and crystals (OI-P)																	
n	83	103	51	105	43	67	78	140	66	258	248	251	264	305	205	89	110
3D min.	1.0	1.0	1.0	1.0	1.0	1.0	1.0	1.0	1.0	1.0	1.0	1.0	1.0	1.0	1.0	1.0	1.0
int.	1.1	1.0	1.1	1.4	1.4	1.2	1.2	1.2	1.1	1.1	1.1	1.2	1.1	1.1	1.2	1.2	1.2
maj. exes	1.4	1.3	1.3	1.5	1.6	1.3	1.5	1.3	3.0	1.7	1.5	1.5	1.5	1.6	1.2	1.9	1.7
R ²	0.86	0.72	0.82	0.89	0.74	0.77	0.84	0.82	0.66	0.82	0.86	0.84	0.73	0.72	0.76	0.72	0.71
Max 2D elongation*	1.7	2.2	1.9	2.1	2.0	2.2	2.5	2.5	4.3	2.5	2.5	3.4	3.4	4.0	3.2	3.6	3.0

OI-RC = recrystallized OI; OI-P = peritectic OI formed after amphibole (Amp), orthopyroxene (Opx), and phlogopite (Phl); OI-PM = primary magmatic OI; P = polyhedral; D = dendritic; E = elongated. n = number of analyses; σ = standard deviation; *d* = standard error ($2\sigma/n^{1/2}$). min = minor, int = intermediate, and maj = major axes. * Max 2D elongation, i.e. "maximum" major/minor axial ratios were determined using the ten largest values derived from our image analysis

Table 4: Summary of characteristic textures and their proposed potential to distinguish olivine of recrystallized, peritectic, and primary magmatic origins

Olivine types	<i>Secondary magmatic olivine</i>	<i>Primary magmatic olivine</i>	<i>Textural potential</i>
	<i>Dendritic, recrystallized olivine</i>	<i>Dendritic, primary olivine (OI-PM)</i>	
Crystal size	Small to large	Small to large	*
Inclusions	Fluid, glass, minerals possible	Fluid, glass, minerals possible	*
Crystal shape	Euhedral to highly irregular	Elongated, possibly irregular	**
Branch shape	Short prismatic	Elongated prismatic to tabular	***
Elongation of crystals and main dendritic branches	Parallel to oblique, commonly oblique for recrystallized crystal fragments	Commonly parallel, oblique for highly elongated branches	**
Olivine types	<i>Peritectic, polyhedral olivine</i>	<i>Primary magmatic, polyhedral olivine</i>	<i>Textural potential</i>
Crystal size	Small to large	Small to large	*
Inclusions	Fluid, glass, minerals possible	Fluid, glass, minerals possible	**
Crystal shape	Euhedral-subhedral, short prismatic to elongated	Euhedral-subhedral, short prismatic to elongated	*
Cluster shape	Highly irregular, commonly crystal-poor cores	Highly irregular, commonly crystal-rich cores	**
Crystal orientation in clusters	Subradial to random, crystals rarely touch in center of clusters	Subradial to random, crystals commonly touch in center of clusters	**

Textures with low (*) to high (***) estimated potential to distinguish olivine of different origins